TECH LIBRARY KAFB, NM
0061265

NASA CONTRACTOR REPORT

NASA CR-
c.1
LOAN COPY: RET
AFWL (DOUL)
KIRTLAND AFB, N. M.

NASA CR-2003

PREDICTION OF UNSTEADY AERODYNAMIC LOADINGS CAUSED BY TRAILING EDGE CONTROL SURFACE MOTIONS IN SUBSONIC COMPRESSIBLE FLOW — ANALYSIS AND RESULTS

by W. S. Rowe, B. A. Winther, and M. C. Redman

Prepared by
THE BOEING COMPANY
Renton, Wash.
for Langley Research Center

NATIONAL AERONAUTICS AND SPACE ADMINISTRATION • WASHINGTON, D. C. • JUNE 1972

TECH LIBRARY KAFB, NM

0061265

1. Report No.	2. Government Accession No.	3. Recipient's Catalog No.
NASA CR-2003		

4. Title and Subtitle	5. Report Date
PREDICTION OF UNSTEADY LOADINGS CAUSED BY TRAILING EDGE CONTROL SURFACE MOTIONS IN SUBSONIC COMPRESSIBLE FLOW - - ANALYSIS AND RESULTS	June 1972
	6. Performing Organization Code
7. Author(s)	8. Performing Organization Report No.
W. S. Rowe, B. A. Winther, and M. C. Redman	
	10. Work Unit No.
9. Performing Organization Name and Address	114-08-05-02
The Boeing Company	11. Contract or Grant No.
Renton, Wash.	NAS1-10536
	13. Type of Report and Period Covered
12. Sponsoring Agency Name and Address	Contractor Report
National Aeronautics and Space Administration Washington, D.C.	14. Sponsoring Agency Code

15. Supplementary Notes

16. Abstract

A theoretical analysis and computer program have been developed for the prediction of unsteady lifting surface loadings caused by motions of trailing edge control surfaces having sealed gaps. The final form of the downwash integral equation has been formulated by isolating the singularities from the non-singular terms and establishing a preferred solution process to remove and evaluate the downwash discontinuities in a systematic manner. Comparisions of theoretical and experimental pressure data are made for several control surface configurations. The comparisions indicate that reasonably accurate theoretical pressure distributions and generalized forces may be obtained for a wide variety of control surface configurations.

Spanwise symmetry or antisymmetry of motion, and up to four control surfaces on each half span can be accommodated.

17. Key Words (Suggested by Author(s))	18. Distribution Statement
Flutter, Wing-Control-Surface Flutter, Aeroelasticity, Structural Dynamics, Aerodynamics, Unsteady Aerodynamics	Unclassified-Unlimited

19. Security Classif. (of this report)	20. Security Classif. (of this page)	21. No. of Pages	22. Price*
Unclassified	Unclassified	76	$3.00

*For sale by the National Technical Information Service, Springfield, Virginia 22151

CONTENTS

PREDICTION OF UNSTEADY AERODYNAMIC LOADINGS CAUSED BY TRAILING EDGE CONTROL SURFACE MOTIONS IN SUBSONIC COMPRESSIBLE FLOW--ANALYSIS AND RESULTS

By

W. S. ROWE, B. A. WINTHER, and M. C. REDMAN
THE BOEING COMPANY

SUMMARY

A theoretical analysis and computer program have been developed for the prediction of unsteady lifting surface loadings caused by motions of trailing edge control surfaces having sealed gaps. The final form of the downwash integral equation has been formulated by isolating the singularities from the non-singular terms and establishing a preferred solution process to remove and evaluate the downwash discontinuities in a systematic manner. Comparisions of theoretical and experimental pressure data are made for several control surface configurations. The comparisions indicate that reasonably accurate theoretical pressure distributions and generalized forces may be obtained for a wide variety of control surface configurations.

INTRODUCTION

Historically, much effort has been expended to adapt conventional oscillating lifting-surface solution techniques to wings with control surfaces. Extensive use has been made of the reverse flow theorem (reference 1) to construct an analytical upwash function that is used in reverse flow to produce "equivalent" generalized forces. The generated upwash function is obtained by the expedient of smoothing over, in one way or another, the slope discontinuities and corresponding singularities within the pressure functions. The "equivalent" upwash function does not match the control surface slope accurately at all points but does produce reasonable "indirect" generalized forces. The usefulness of this method deteriorates when the 'direct' hinge-moment term is to be determined.

The work of reference 2 is one of the few subsonic methods developed to determine the 'direct' surface loadings using pressure terms that are capable of correctly representing the known singularity functions around the boundaries of the control surface. However, it was found that solutions obtained from the method of reference 2 were highly sensitive to the relative location and number of control point collocation stations used in the analysis. The sensitivity may be attributed to the particular solution process being applied that assumes that discontinuous downwash distributions may be approximated by a linear combination of polynomial represented downwash sheets that satisfy the boundary conditions at a select set of control points. Changing the control point locations by relatively small amounts results in large changes in the unsteady loadings, consequently the method requires calculation of downwashes at many stations and seeking solutions in a least-squares-error sense.

Solution sensitivity remained until pressure distributions were developed (reference 3) that identify the functional distribution and singularity strengths required to produce identical mathematical downwash discontinuities contained in the kinematic distribution. A preferred solution process was developed by subtracting the discontinuous mathematical downwash distribution from the discontinuous kinematic distribution resulting in smooth downwash distribution for which standard lifting-surface solutions could be applied. The resulting loadings would then be relatively insensitive to the locations and number of control points used in the analysis.

The present work represents an extension of the analytical methods suggested in reference 3 to provide a capability of numerically predicting the unsteady loadings caused by control surface motions that is relatively insensitive to locations of collocation stations on the surface. Documentation of the computer program design, usage, and limitations is provided in reference 4.

SYMBOLS

All quantities are dimensionless except as indicated

a_{nm}		Unknown coefficient of assumed pressure modes, equation 54
b	[length]	Local semichord
b_o	[length]	Reference length
$\bar{c}$		Local chord length nondimensional with respect to b_o
$f_r(\eta)$		Regular spanwise pressure difference distribution, equation 55
$f_s(\eta)$		Singular spanwise pressure difference distribution, equations 38a and 47.
$g_r(\xi,\eta)$		Regular chordwise pressure difference distribution, equation 56
$g_s(\xi,\eta)$		Singular chordwise pressure difference distribution, equations 39 and 47
$H_j(x,y)$		Mode shape of mode j, $\bar{H}_j(x,y)b_o$
i		$\sqrt{-1}$
$K(x,\xi,y,\eta)$		Kernel function, equation 6
k		Reduced frequency = $\frac{\omega b_o}{V}$
M		Mach number
P_ℓ	[Force/area]	Pressure on lower surface
P_u	[Force/area]	Pressure on upper surface
q_j		Generalized coordinate amplitude for mode j
Q_{ij}		Generalized forces (see equation 84 for dimensions)
Q^s_{ij}		Sectional generalized forces (see equation 82 for dimensions)
R		$\sqrt{x_o^2 + \beta^2 y_o^2}$
S	[length]	Semispan
s		Nondimensional semispan, S/b_o
V	[length/time]	Free stream velocity
$\frac{w}{V}$		Kinematic angle of attack or nondimensional normalwash
$\bar{w}$		$\frac{\bar{w}}{V}$
$\bar{w}_j$		$w_j/q_j e^{i\omega\tau}$

X,Y,Z	[length]	Dimensional Coordinates
x,y,z		Coordinates nondimensional with respect to b_o
$\underline{x}$		$(x - x_m)/(b/b_o)$
$\overline{x}$		$x - x_\ell$
x_c		Nondimensional coordinate of the control surface hingeline
x_m		Nondimensional coordinate of the mid-chord line
x_ℓ		Nondimensional coordinate of the leading edge
x_t		Nondimensional coordinate of the trailing edge
x_o		$x - \xi$
y_o		$y - \eta$
β		$\sqrt{1 - M^2}$
$\beta_{h\ell}$		$\sqrt{\beta^2 + \tan^2 \Lambda_c}$
δ	[radian]	Hingeline rotation angle measured in the plane perpendicular to hingeline and positive trailing edge down
ΔC_p		Nondimensional steady state pressure difference between lower and upper surfaces, $(P_\ell - P_u)/(\rho V^2/2)$
$\Delta C_p'$		In-phase part of the nondimensional pressure difference
$\Delta C_p''$		Out-of-phase part of the nondimensional pressure difference
Λ_c	[radian]	Sweep angle of the control surface hingeline, positive swept back
ξ,η,ζ		Dummy variables for (x,y,z)
$\overline{\xi},\overline{\eta},\overline{\zeta}$		Scaled dummy variables (see equation (30))
$\Theta(\eta)$	[radian]	Rotation angle of control surface hingeline at (η), measured in the plane perpendicular to the y-axis and positive trailing edge up
ρ	[mass/length^3]	Density of the fluid
τ	[time]	Time
ω	[1/time]	Circular frequency of oscillation
ω^*		Reduced frequency = k

ANALYTICAL FORMULATION

The Integral Equation and its Elements

The purpose of this report is to describe the procedures used in calculating the generalized aerodynamic forces existing on a lifting surface caused by control surface motions in subsonic flow. The analysis is applicable to planform configurations having full span or multiple partial span control surfaces located anywhere along the planform trailing edge.

A typical partial span control surface configuration is shown in figure 1 where the analysis coordinate system is defined.

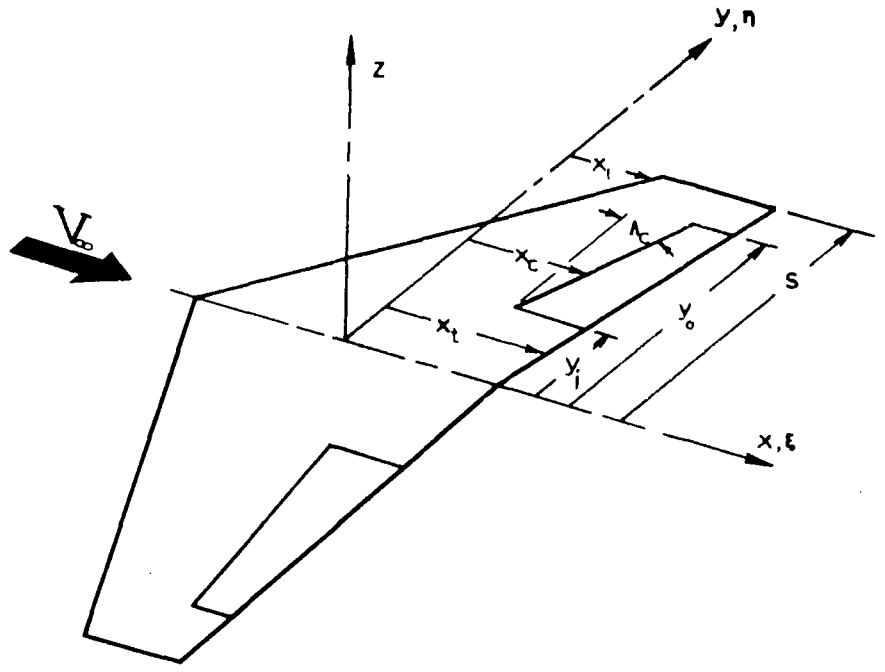

Figure 1.—Coordinate System Definition

Solutions are obtained through an evaluation of the downwash-pressure integral equation that has been derived from the linearized potential equation (1).

$$\nabla^2\Phi(x,y,z,t) - \frac{1}{a^2}\left(V\frac{\partial}{\partial x} + \frac{\partial}{\partial t}\right)^2 \Phi(x,y,z,t) = 0 \qquad (1)$$

The downwash-pressure integral equation derived in reference 5 provides the basis for the analytical formulations used in developing numerical methods for predicting unsteady loadings on lifting surfaces.

The form of the integral equation used throughout this discussion is given as:

$$\left[\frac{\bar{w}}{V}\right]_j = \frac{1}{4\pi\rho V^2} \int_{-s}^{s} \int_{x_\ell}^{x_t} \Delta P_j(\xi,\eta)\, K(x,\xi,y,\eta)\, d\xi d\eta \tag{2}$$

Equation (2) has been written using the subscript j to denote that pressure distributions obtained by the solution process will be those necessary to satisfy the boundary conditions of the j^{th} deformation mode shape.

The pressure distribution $\Delta P_j(\xi,\eta)$ is the only unknown function within the equation and is equal to the pressure difference between lower and upper surfaces defined by:

$$\Delta P_j(\xi,\eta) = P_\ell - P_u \tag{3}$$

The kinematic downwash* term $\left[\frac{\bar{w}}{V}\right]_j$ is developed on the basis of the modal representation of the wing deflection Z for sinusoidal motion

$$Z \approx \sum_j H_j(x,y) q_j e^{i\omega\tau} \tag{4a}$$

and is defined as:

$$\left[\frac{w}{V}\right]_j = \left[\frac{\bar{w}}{V}\right]_j q_j e^{i\omega\tau} = -\left[\frac{\partial H_j(x,y)}{b_o \partial x} + i\frac{\omega}{V} H_j(x,y)\right] q_j e^{i\omega\tau} \tag{4b}$$

where $H_j(x,y)$ is the deflection shape of the j^{th} mode and is in the same dimensional units as b_o and q_j is dimensionless.

The subscript (j) is omitted in the remaining sections, up to the section on generalized forces, with the understanding that the pressure terms being determined are those terms necessary to satisfy the j^{th} mode shape boundary conditions.

The $K(x,\xi,y,\eta)$ term represents the kernel function of the integral equation that describes the surface normalwash at (x,y) due to a pulsating pressure doublet located at (ξ,η) defined by:

* kinematic downwash has the opposite positive sense to that of the resulting or caused downwash at the surface.

$$K(x,\xi,y,\eta) = e^{\frac{-i\omega}{v}(x-\xi)} \lim_{z\to 0} \frac{\partial^2}{\partial z^2} \int_{-\infty}^{x-\xi} \frac{e^{\frac{i\omega}{v\beta^2}(\lambda - M\sqrt{\lambda^2+\beta^2(y-\eta)^2+\beta^2z^2})}d\lambda}{\sqrt{\lambda^2+\beta^2(y-\eta)^2+\beta^2z^2}} \qquad (5)$$

Reduction of equation (5) into a form that may be easily evaluated by routine numerical procedures was accomplished by Watkins, Runyan, and Woolston (reference 6) and presented in non-dimensional form by considering the variable as being referenced to some chosen length and introducing the reduced frequency parameter $k = \frac{b_o\omega}{v}$.

$$K(x,\xi,y,\eta) = \frac{e^{-ikx_o}}{y_o^2}\left\{-k|y_o|\left[K_1|ky_o| + i\tfrac{\pi}{2}(I_1|ky_o| - L_1|ky_o|) - i\right.\right.$$
$$\left. -i\int_0^h \tau/(1+\tau^2)^{1/2}\exp(ik|y_o|\tau)\,d\tau\right]$$
$$\left. -x_o/(x_o^2+\beta^2y_o^2)^{1/2}\cdot\exp\frac{ik}{\beta^2}(x_o-M(x_o^2+\beta^2y_o^2)^{1/2})\right\} \qquad (6)$$

where $h = \left(x_o - M(x_o^2+\beta^2y_o^2)^{1/2}\right)/\beta^2y_o$

Equation (6) contains functions that are singular at the downwash control point (x,y) and may cause numerical difficulties in evaluating the integral equation. However, the singularities have been identified and may be isolated in the following form:

$$K(x,\xi,y,\eta) = K_{ns}(x,\xi,y,\eta) + K_s(x,\xi,y,\eta) \qquad (7)$$

where $K_{ns}(x,\xi,y,\eta)$ is the non-singular part of the kernel function

and the singular part is given by

$$K_s(x,\xi,y,\eta) = e^{-ikx_o}\left\{-\frac{1}{y_o^2}\left[1+x_o/(x_o^2+\beta^2y_o^2)^{1/2}\right] + ik/(x_o^2+\beta^2y_o^2)^{1/2}\right.$$
$$\left. -\frac{k^2}{2}\ln\left|(x_o^2+\beta^2y_o^2)^{1/2} - x_o\right| - \frac{k^2}{2\beta^2}\left[x_o/(x_o^2+\beta^2y_o^2)^{1/2} - M\right]\right\} \qquad (8)$$

Insertion of the above definitions into the downwash integral equation results in the following expression to be evaluated over the surface to satisfy the boundary conditions.

$$4\pi\rho V^2\left[\frac{\bar{w}}{V}\right] = \int\int \Delta p(\xi,\eta)K_{ns}(x,\xi,y,\eta)\, d\xi d\eta$$

$$-\int\int \Delta p(\xi,\eta)e^{-ikx_o}\frac{1}{y_o^2}\left[1+x_o/(x_o^2+\beta^2y_o^2)^{1/2}\right]d\xi d\eta$$

$$+ik\int\int \Delta p(\xi,\eta)e^{ikx_o}/(x_o^2+\beta^2y_o^2)^{1/2}\, d\xi d\eta$$

$$-\frac{k^2}{2}\int\int \Delta p(\xi,\eta)e^{-ikx_o}\ln\left|(x_o^2+\beta^2y_o^2)^{1/2}-x_o\right| d\xi d\eta \qquad (9)$$

$$-\frac{k^2}{2\beta^2}\int\int \Delta p(\xi,\eta)e^{-ikx_o}\left[x_o/(x_o^2+\beta^2y_o^2)^{1/2} - M\right]d\xi d\eta$$

The first integral of equation (9) represents the contribution to the downwash at the point (x,y) due to the non-singular part of the kernel function. The general shape of K_{ns} is usually quite smooth for low values of Mach number reflecting the strong sinusoidal characteristics of e^{-ikx_o} in the expression. However, the chordwise characteristics change quite rapidly for Mach numbers greater than M = 0.85 as is demonstrated within figure 2 that shows the chordwise variation in the imaginary part of K_{ns} with Mach number.

The $(x-\xi)$ coordinate of figure 2 represents the chordwise difference between the pulse sending point located at (ξ,η) and the downwash station (x,y).

Since the functional distributions of K_{ns} are quite different forward and aft of the downwash station the chordwise integration interval $x_1 \leq \xi \leq x_t$ is subdivided into two intervals $x_1 \leq \xi \leq x$ and $x \leq \xi \leq x_t$ to provide an accurate evaluation of the chordwise integral.

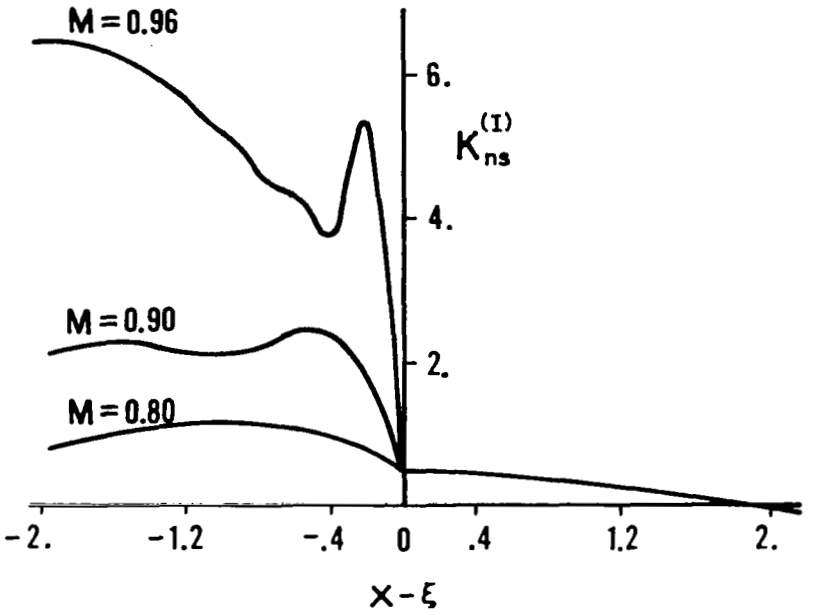

Figure 2.- Chordwise Variation of $K_{ns}^{(I)}$ as a Function of Mach Number for $y-\eta = 0.05$, $k = 0.7854$

The second, third, and fourth integrals of equation (9) represent downwash contribution due to the dipole, square root, and logarithmic singularity terms respectively. The last integral does not contain a singularity in the spanwise direction but does require special means to evaluate its downwash contribution since a finite discontinuity exists for values of $\eta \rightarrow y$.

Evaluation of the Dipole Term

The downwash contribution due to the dipole term is evaluated using the method suggested by Hsu (reference 7). The dipole integral of equation (9) is given as

$$\bar{w}^{dp} = -\int_{-s}^{s}\int_{x_\ell}^{x_t} \Delta p(\xi,\eta) e^{-ikx_o} \frac{1}{(y-\eta)^2}\left[1 + (x-\xi)/\left[(x-\xi)^2+\beta^2(y-\eta)^2\right]^{1/2}\right] d\xi d\eta \quad (10)$$

where the form of equation (10) is obtained by developing the dipole expression from a different viewpoint than taken by Hsu.

The dipole portion of the kernel function is developed by considering the normalwash at a point (x,y,ε) that is located just off of the surface shown in figure 3.

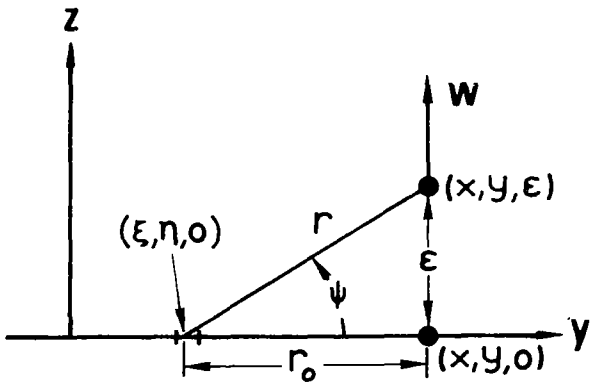

Figure 3.- Coordinate System Used in the Kernel Function Derivation

The kernel function describing the normalwash at (x,y,ε) due to a pressure pulse at (ξ,η,o) is given by

$$K_W = -e^{-ikx_o}\left[\frac{1}{r}\frac{\partial E_o}{\partial r} + \sin^2\psi\left(\frac{\partial^2 E_o}{\partial r^2} - \frac{1}{r}\frac{\partial E_o}{\partial r}\right)\right] \tag{11}$$

where

$$E_o = \int_{-\infty}^{h} e^{ik\lambda}\,(r^2 + \lambda^2)^{-1/2}\,d\lambda$$

$$h = 1/\beta^2\,[x_o - MR],\quad R = (x_o^2+\beta^2 r^2)^{1/2} \text{ and } x_o = x - \xi$$

The dipole portion of K_W is given by

$$K_W^{dp} = -e^{-ikx_o}\frac{1}{r^2}(1 + x_o/R)(-1 + 2\sin^2\psi) \tag{12}$$

and may be put in a different form by using the geometric properties of figure 3 given as:

$r^2 = r_o^2 + \varepsilon^2$; $r_o = y_o = y - \eta$ and $\sin\psi = \frac{\varepsilon}{r}$; $R_o = (x_o^2+\beta^2 r_o^2)^{1/2}$

Then K_W^{dp} takes on the definition

$$K_w^{dp} = e^{-ikx_o} \frac{r_o^2 - \varepsilon^2}{(r_o^2+\varepsilon^2)^2} [1 + \frac{x_o}{R_o} + O(\varepsilon^2)] \tag{13}$$

where the terms represented by $O(\varepsilon^2) \rightarrow 0$ as $\varepsilon \rightarrow 0$

The normalwash at (x,y,0) is obtained by a limiting process allowing $\varepsilon \rightarrow 0$ after the normalwash integral has been evaluated as indicated by the following:

$$w^{dp}(x,y,0) = \lim_{\varepsilon \rightarrow 0} \int_{-s}^{s} \frac{(y_o^2-\varepsilon^2)(s^2-\eta^2)^{1/2}}{(y_o^2+\varepsilon^2)^2} \int_{x_\ell}^{x_t} \frac{\Delta p(\xi,\eta)}{(s^2-\eta^2)^{1/2}} e^{-ikx_o(1+\frac{x_o}{R_o})} \, d\xi d\eta \tag{14}$$

Following the development of reference 7, let $G(x,y,\eta)$ be the value of the chordwise integral at

$$G(x,y,\eta) = \int_{x_\ell}^{x_t} \frac{\Delta p(\xi,\eta)}{(s^2-\eta^2)^{1/2}} e^{-ikx_o} (1 + x_o/R_o) \, d\xi \tag{15}$$

as $\eta \rightarrow y$ this becomes

$$\lim_{\eta \rightarrow y} G(x,y,\eta) = G(x,y,y)$$

Then one of the singularities is subtracted from equation (14) to provide the expression

$$w^{dp}(x,y,0) = \lim_{\varepsilon \rightarrow 0} \left[\int_{-s}^{+s} y_o \frac{(y^2-\eta^2)(s^2-\eta^2)^{1/2}}{(y_o^2+\varepsilon^2)^2} \left[\frac{G(x,y,\eta) - G(x,y,y)}{(y-\eta)}\right] d\eta + G(x,y,y) \int_{-s}^{s} (y_o^2-\varepsilon^2)(s^2-\eta^2)^{1/2}/(y_o^2+\varepsilon^2)^2 \, d\eta \right] \tag{16}$$

The finite part of the second integral is given as:

$$\lim_{\varepsilon \rightarrow 0} \int_{-s}^{s} (y_o^2-\varepsilon^2)(s^2-\eta^2)^{1/2}/(y^2+\varepsilon^2)^2 \, d\eta = -\pi$$

Evaluation of the first integral would still have to be accomplished by the use of Cauchy integrals, however this can be circumvented by subtracting an additional singularity.

Define $H(x,y,\eta) = (s^2 - \eta^2)[G(x,y,\eta) - G(x,y,y)]/(y-\eta)$ (17)

and let

$$H(x,y,y) = \lim_{\eta \to y} (s^2 - \eta^2) \frac{[G(x,y,\eta) - G(x,y,y)]}{y - \eta} \tag{17-A}$$

$$= -(s^2 - y^2)G'(x,y,y) = -(s^2 - y^2) \frac{\partial}{\partial \eta}\left[G(x,y,\eta)\right]_{\eta=y}$$

then

$$w^{dp}(x,y,0) = \lim_{\varepsilon \to 0}\left[\int_{-s}^{s} y_o^2 \frac{y_o^2 - \varepsilon^2}{(y_o^2 + \varepsilon^2)^2} \frac{1}{(s^2 - \eta^2)^{1/2}} \frac{H(x,y,\eta) - H(x,y,y)}{y - \eta} d\eta \right. \tag{18}$$

$$\left. + H(x,y,y) \int_{-s}^{s} y_o \frac{y_o^2 - \varepsilon^2}{(y_o^2 + \varepsilon^2)^2} \frac{1}{(s^2 - \eta^2)^{1/2}} d\eta \right] - \pi G(x,y,y)$$

The second integral of equation (18) becomes equal to zero as $\varepsilon \to 0$ and finally the dipole downwash term takes on the integrable form of

$$w^{dp}(x,y,0) = \int_{-s}^{s} \frac{1}{(s^2 - \eta^2)^{1/2}}\left[(s^2 - \eta^2) \frac{[G(x,y,\eta) - G(x,y,y)]}{(y - \eta)^2} \right. \tag{19}$$

$$\left. - \frac{(s^2 - y^2)\, G'(x,y,y)}{y - \eta}\right] d\eta - \pi G(x,y,y)$$

It should be noted that, as $\eta \to y$, the integrand of equation (19) tends to take on the definition of a second derivative of $G(x,y,\eta)$ with respect to η. However, the second derivative does not exist since the integrand is singular at the downwash chord $\eta = y$. Figure 4 represents a plot of the spanwise distribution of the integrand $I(y,\eta)$ of equation (19) and displays the singularity existing at the downwash chord. The analysis was accomplished using an assumed pressure distribution made up of a single sine wave in both the chordwise and spanwise directions. Location of the collocation station for which the plotted values apply is as shown in the planform sketch having coordinates of $\underline{Y} = y/s = 0.35$ and $\underline{x} = -0.766$.

$\underline{x}$ is defined as a decimal fraction of the downwash half chord and

given as $\underline{x} = \dfrac{(x - x_m)\, b_o}{b(y)}$

where x_m is the x coordinate of the mean chord line and

$b(y)$ is the half chord value of the downwash chord.

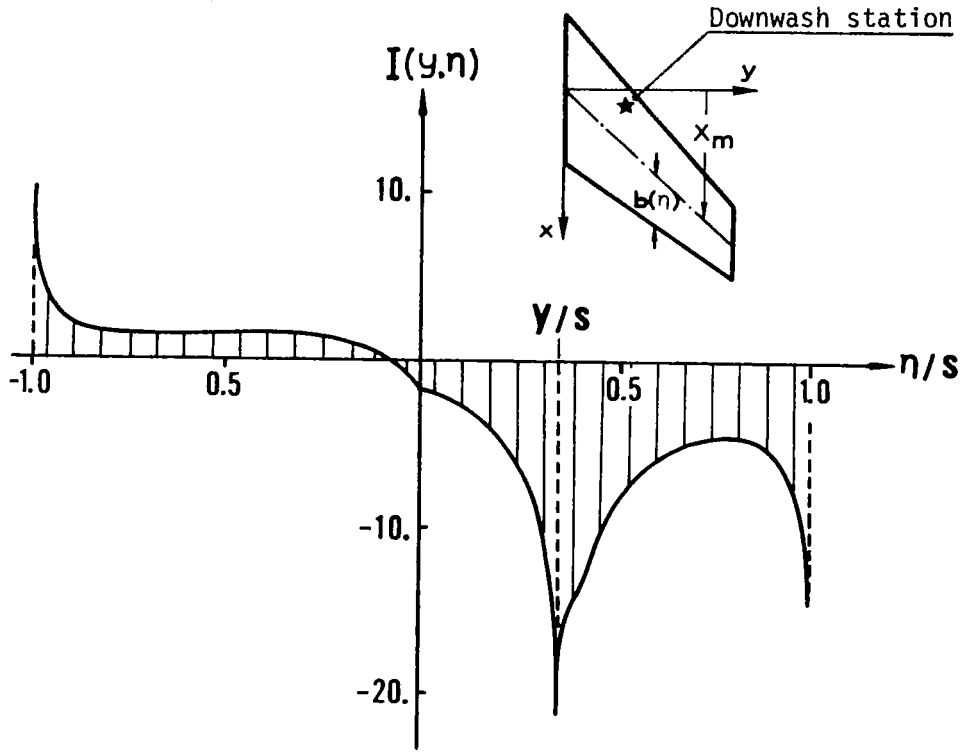

Figure 4.- Spanwise Variation of the Integrand of Equation (19) Displaying the Singularity at the Downwash Chord

In the following section, the singularity just described is identified as being logarithmic in its distribution and consequently, numerical evaluation of equation (19) will be accomplished using quadrature formulas appropriate for evaluating logarithmic singular functions. Also, the following section contains a description of how the spanwise distribution of the integrand may be modified to provide a non-singular distribution that may be readily evaluated by Legendre-Gauss integration quadrature formulas.

Identification of Spanwise Singularities

The spanwise singularity, observed within the above integral evaluation of the dipole term, was first identified by Multhopp (reference 8) within the development of the steady state lifting surface solution. The method applied to identify the singularity for the steady state case has been extended by Laschka (reference 9) to include the unsteady case.

The functional expression of the dipole singularity may be obtained by developing a Taylor series expansion of $\Delta P(\xi,\eta)\, e^{-ikx_o}$ about the downwash station and performing the resulting chordwise integrations. That is, we let $\Delta P(\xi,\eta)\, e^{-ikx_o}$ be approximated by the Taylor series given by:

$$\Delta P(\xi,\eta)\, e^{-ik(x-\xi)} = \Delta P(\xi,y)\, e^{-ik(x-\xi)} + (\eta-y)\left[\frac{\partial}{\partial\eta}\Delta P(\xi,\eta)\, e^{-ik(x-\xi)}\right]_{\eta=y} + \ldots \tag{20-A}$$

then develop expansions of the individual terms

$$\Delta P(\xi,y)\, e^{-ik(x-\xi)} = \Delta P(x,y) + (\xi-x)\left[\frac{\partial}{\partial\xi}\Delta P(\xi,y)\, e^{-ik(x-\xi)}\right]_{\xi=x} + \ldots \tag{20-B}$$

$$\left[\frac{\partial}{\partial\eta}\Delta P(\xi,\eta)\, e^{-ik(x-\xi)}\right]_{\eta=y} = \left[\frac{\partial\Delta P(\xi,\eta)}{\partial\eta}\right]_{\substack{\eta=y\\ \xi=x}} + (\xi-x)\left[\frac{\partial}{\partial\xi}\,\frac{\partial}{\partial\eta}\Delta P(\xi,\eta)\, e^{-ik(x-\xi)}\right]_{\eta=y,\ \xi=x} + \ldots \tag{20-C}$$

Inserting equations (20-B) and (20-C) into (20-A) produces a spanwise and chordwise Taylor series approximation of $\Delta P(\xi,\eta)\, e^{-ikx_o}$ given by

$$\Delta P(\xi,\eta)\, e^{-ik(x-\xi)} = \Delta P(x,y) + (\eta-y)\left[\frac{\partial}{\partial\eta}\Delta P(\xi,\eta)\right]_{\substack{\eta=y\\ \xi=x}} + (\xi-x)\left[\frac{\partial}{\partial\xi}\Delta P(\xi,y)\, e^{-ik(x-\xi)}\right]_{\xi=x} + (\eta-y)\left[\frac{\partial^2}{\partial\xi\partial\eta}\Delta P(\xi,\eta)\, e^{-ik(x-\xi)}\right]_{\substack{\eta=y\\ \xi=x}} + \ldots \tag{20-D}$$

The singularity expression is obtained by insertion of equation (20-D) into the chordwise integral and performing the integration that results in

$$I^{dp} = -\int_{-s}^{s} \frac{1}{(y-\eta)^2}\Bigg[\Bigg\{\Bigg[\frac{\partial}{\partial\xi}\Delta P(\xi,y)\, e^{-ik(x-\xi)}\Bigg]_{\xi=x} + \tag{21}$$

$$-(y-\eta)\Bigg[\frac{\partial}{\partial\xi\partial\eta}\Delta P(\xi,\eta)\, e^{-ik(x-\xi)}\Bigg]_{\substack{\eta=y\\ \xi=x}}\Bigg\}\cdot$$

$$\cdot\left\{\frac{\beta^2}{2}(y-\eta)^2 \ln\beta^2(y-\eta)^2\right\} + \text{Regular Terms}\Bigg]\, d\eta$$

Thus the dipole term contains the recognizable dipole singularity along with an additional logarithmic singularity at the spanwise downwash station.

Part of the "regular terms" of the second expression in equation (21) are composed of terms that are expressible as

$$(y-\eta)^4 \ln\beta^2(y-\eta)^2 \quad , \ldots\ldots \quad (y-\eta)^{2n} \ln\left[\beta^2(y-\eta)^2\right]$$

that are continuous not requiring special attention in evaluating the spanwise integral.

The third integral of equation (9) also contains a spanwise singularity that is proportional to $\ln|y-\eta|$ that is identified by an insertion of the Taylor series of equation (20-D) into the integral and performing the indicated chordwise integration.

The resulting spanwise integral is then given by:

$$I^{(3)}(y) = ik\int_{-s}^{s}\Bigg[\Bigg\{\Delta P(x,y) + (\eta-y)\Bigg[\frac{\partial\Delta P(\xi,\eta)}{\partial\eta}\Bigg]_{\substack{\eta=y\\ \xi=x}}\Bigg\}\cdot \tag{22}$$

$$\cdot\left\{\ln\beta^2(y-\eta)^2\right\} + \text{Regular Terms}\Bigg]\, d\eta$$

Again, part of the "regular terms" contain expressions that are proportional to

$$(y-\eta)^2 \ln\beta^2(y-\eta)^2, \ldots\ldots (y-\eta)^{2n} \ln\beta^2(y-\eta)^2$$

which are continuous and do not require special integration procedures to evaluate the spanwise integral.

Following a similar line of thought, it can be shown that the fourth integral of equation (9) is also singular at the spanwise downwash station having the form of:

$$I^{(4)}(y) = -\frac{k^2}{2}\int_{-s}^{s}\left\{ \ln\beta^2(y-\eta)^2 \int_{x_1}^{x} \Delta P(\xi,y)\, e^{-ik(x-\xi)}\, d\xi + \right.$$
$$\left. + \text{ Regular Terms} \right\} d\eta \qquad (23)$$

Once the singularities have been determined they may be subtracted out of the integrand and analytically evaluated outside of the integral.

Figure 5 shows the very smooth spanwise distribution of the integrand $I(y,\eta)$ obtained for the dipole term by subtracting out the identifiable singularities of equation (21). Removal of the singularities allows the use of Legendre-Gauss quadrature formulas to evaluate the spanwise integral using only a very small number of quadrature stations.

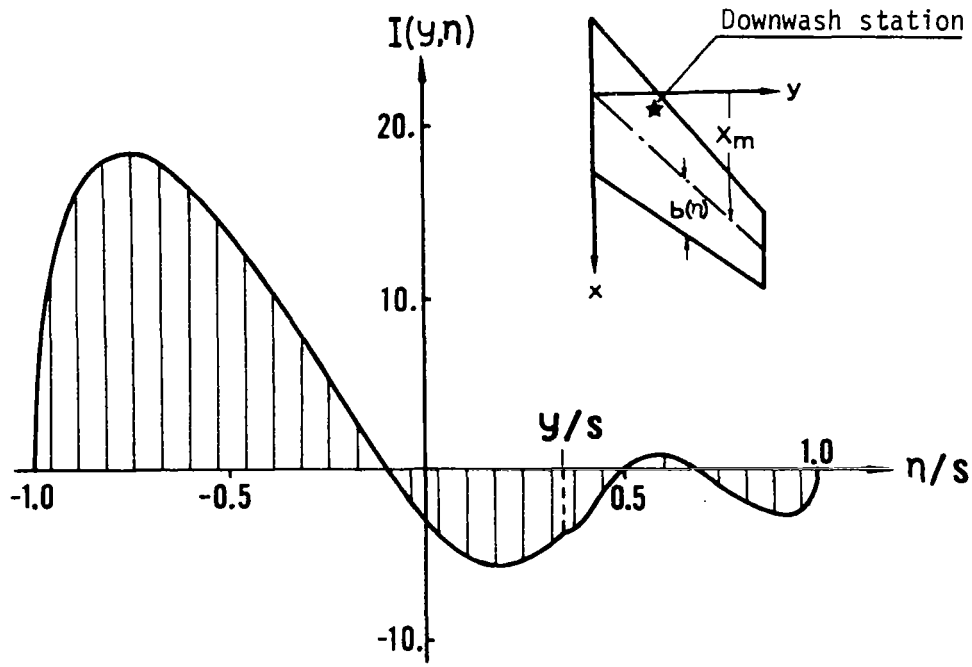

Figure 5.- Spanwise variation of Integrand of Equation (19) with Singularities of Equation (21) removed from the Integrand.

As a consequence of the above there are several options open to the analyst in evaluating the spanwise portions of the downwash integrals and are: (1) ignore the logarithmic singularity since it is of relatively low power, (2) subtract the singularities out of the expression and analytically evaluate their downwash contribution, and (3) apply numerical integration quadrature functions that can evaluate the logarithmic term at the downwash chord.

Numerical investigations have been performed to determine the validity in using any one of the three integration options within the control surface program. The analysis planform shown in figure 6 is a rectangular wing having a full span flap deflected in steady flow. The deflection shape and step function downwash distribution are also displayed to show the discontinuity that must be matched by the mathematical downwash calculation of the integral equation. The assumed pressure distribution used in the analysis is composed of a chordwise singularity term $\ln(\xi-x_c)^2$ and other modifying terms required to produce the discontinuity in downwash across the hingeline as well as satisfying the boundary conditions along the planform edges.

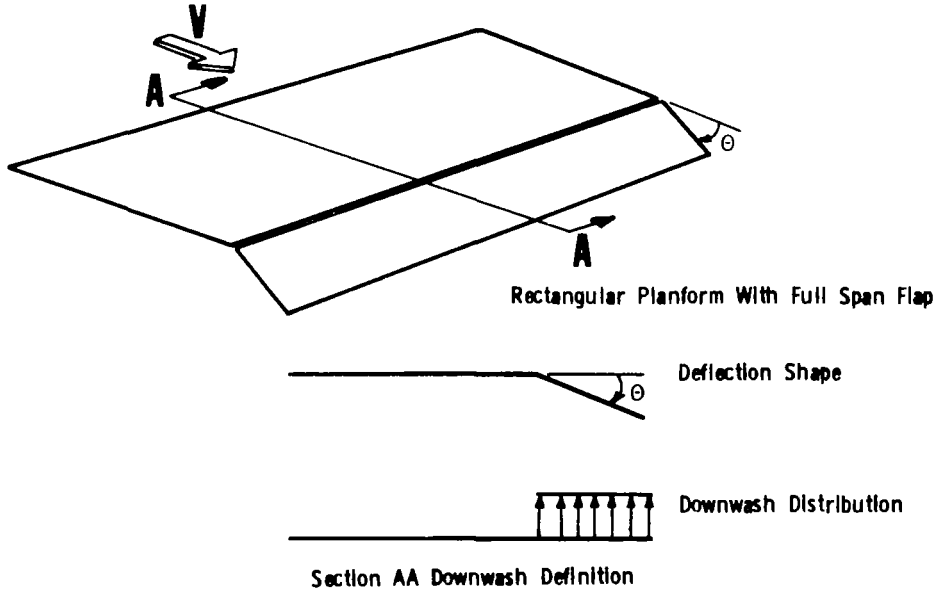

Figure 6.- Analysis Planform Used to Evaluate Effect of Spanwise Singularities on Downwash Distribution

Results of applying option(1) to evaluate the spanwise integral of equation 19 are shown in figure 7. The integral is evaluated using the interdigiting process suggested in reference 7 where a single Gauss-Mehler quadrature function is applied over the complete span of the planform. The singularity at the downwash chord is not recognized by this integration procedure and consequently the resulting chordwise downwash distribution is smooth and continuous across the hingeline. It appears that lifting surface solutions obtained using option(1) will not provide a satisfactory mathematical representation of the boundary conditions for the physical wing-control surface combination.

$$W^{(1)} = \sum_{i}^{I} H_i \left[(s^2 - \eta_i^2) \frac{G(x,y,\eta_i) - G(x,y,y)}{(y - \eta_i)^2} \right] + \pi G(x,y,y)$$

$$H_i = \pi / I \qquad \eta_i = \cos \frac{2i-1}{2I} \pi$$

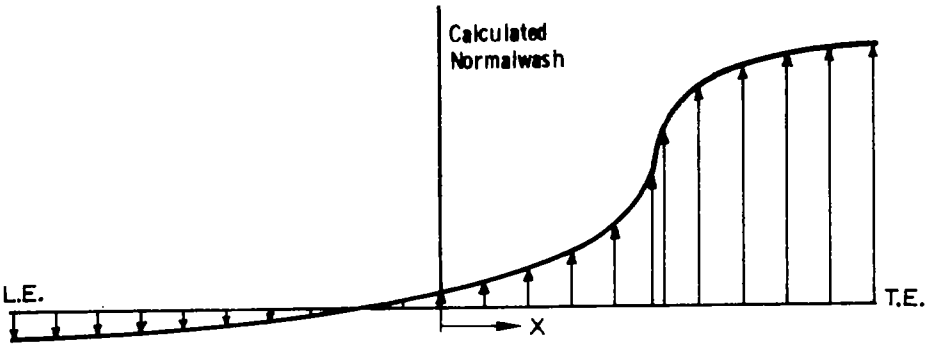

Figure 7.- Chordwise Downwash Distribution at Mid-Span Station Resulting from Applying Option (1) (logarithmic singularity ignored)

Figure 8 presents the results using the second option where the singularity is treated by approximating the pressure terms by a Taylor series expansion and removing the singularity from the spanwise integrand. Equation (19) has been modified by subtracting the singularities (identified in equation (21)) and evaluating their effect outside of the integral as indicated by the downwash equation shown in figure 8.

The downwash distribution appears to be reasonable at large distances from the hingeline, however, the downwash becomes singular at the hingeline. This is to be expected since the pressure term used in the analysis to provide the step function change in boundary conditions across the hingeline is proportional to $\ln|\xi-x_c|$, which cannot be approximated by a Taylor series in the vicinity of the singularity at $\xi = x_c$.

$$W^{(1)} = -\int_{-s}^{s} \frac{1}{\sqrt{s^2-\eta^2}} \left[(s^2-\eta^2) \frac{G(x,y,\eta)-G(x,y,y)}{(y-\eta)^2} - (s^2-y^2)\frac{G'(x,y,y)}{y-\eta} \right.$$

$$\left. + \frac{\beta^2}{2} \frac{\partial}{\partial \xi}\left[\Delta P(\xi,y)\, e^{-ik(x-\xi)}\right]_{\xi=x} \ln\beta^2(y-\eta)^2 \right] d\eta$$

$$+ \frac{\beta^2}{2}\left[\frac{\partial}{\partial \xi}\left[\Delta P(\xi,y)\, e^{-ik(x-\xi)}\right]_{\xi=x}\right] \int_{-s}^{s} \ln\beta^2(y-\eta)^2 d\eta + \pi G(x,y,y)$$

Use single quadrature spanwise plus exact evaluation

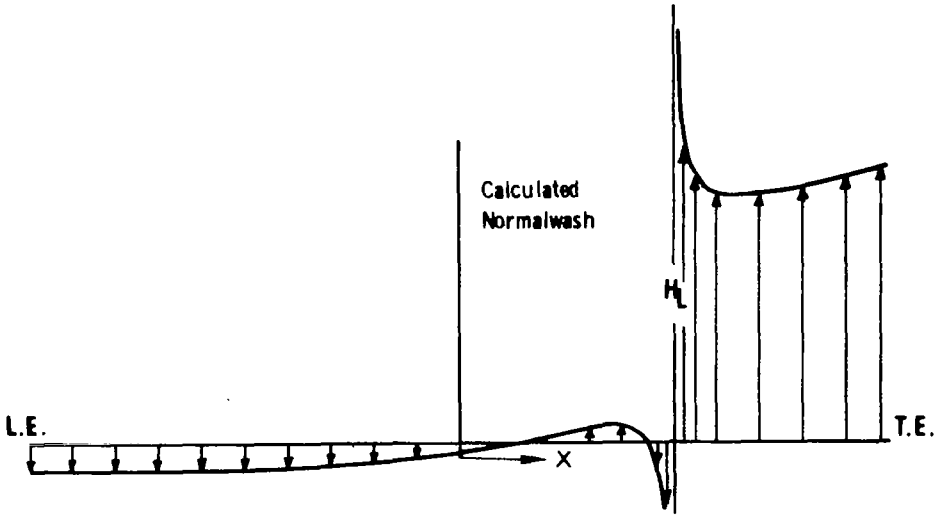

Figure 8.- Chordwise Downwash Distribution Resulting from Applying Option (2) (logarithmic singularity is subtracted and evaluated separately)

The downwash distribution shown in figure 8 indicates that the downwash collocation stations are to be restricted to chordwise locations that are spaced well away from hingeline where large downwash gradients are developed. This restriction may not be satisfied for analyses of wings having small percent chord control surfaces. Large gradients may exist over the chordwise length of small percent chord control surface

and the resulting solutions would be highly dependent upon the number and relative locations of the downwash collocation stations.

This restriction may be removed by applying Option (3) where the spanwise integral is evaluated by subdividing the integration interval, $-s \leq \eta \leq s$, into several subintervals and applying quadrature formulas appropriate to the functional characteristics of the integrand.

Results of applying option (3) to evaluate equation (19) are shown in figure 9. The integration interval has been divided into subregions and appropriate quadrature formulas have been applied in the subregions, i.e., square root quadrature formulas applied at ends of the interval, logarithmic quadrature formulas used on either side of the downwash station, and Legendre quadratures applied within the remaining integration intervals.

$$w^{(1)} = -\left\{\underbrace{\int_{-s}^{l_1} C(\eta)d\eta}_{\text{sq·root}} + \cdots + \underbrace{\int_{l_i}^{l_{i+1}} C(\eta)d\eta}_{\text{log·}} + \cdots \underbrace{\int_{y-\varepsilon}^{y} C(\eta)d\eta}_{\text{log·}} + \underbrace{\int_{y}^{y+\varepsilon} C(\eta)d\eta}_{\text{log·}} + \cdots \underbrace{\int_{s-\gamma}^{s} C(\eta)d\eta}_{\text{sq·root}}\right\} + \pi G(x,y,y)$$

where

$$C(\eta) = \frac{1}{\sqrt{s^2-\eta^2}}\left[(s^2-\eta^2)\,\frac{G(x,y,\eta)-G(x,y,y)}{(y-\eta)^2} - (s^2-y^2)\,\frac{G'(x,y,y)}{(y-\eta)}\right]$$

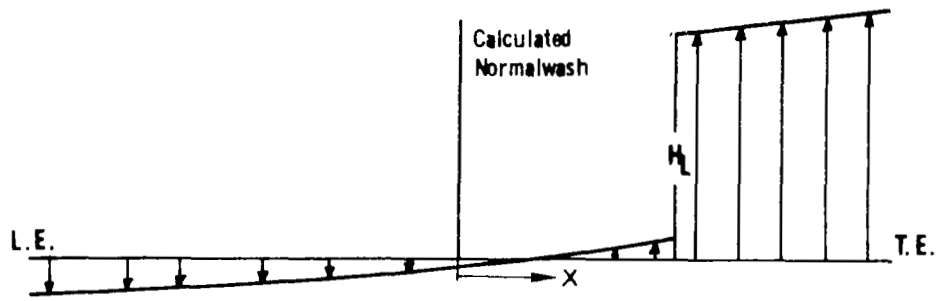

Figure 9.- Chordwise Downwash Distribution Resulting from Applying Option (3) (logarithmic singularity evaluated by appropriate Quadrature Formulas)

The resulting downwash distribution (figure 9) does contain the step function change across the hingeline necessary to satisfy the boundary conditions and does not exhibit any large gradients near the hingeline. Consequently, solutions obtained using option (3) should not be sensitive to

the relative locations of downwash collocation stations even when applied to analysis of small percent chord control surface configurations.

As a consequence of the above, option (2) will be applied to evaluate downwash distributions due to continuous pressure distributions for which a meaningful Taylor series expansion may be developed within small regions around the downwash station. Also, option (3) will be applied to evaluate the downwash distributions due to singular pressure distributions for which a Taylor series approximation of the pressure expression does not exist at the discontinuity stations.

Preferred Solution Process

No direct means is available to obtain a closed form solution of the downwash integral equation that satisfies the boundary conditions exactly everywhere on the surface. Approximate solutions are used in lieu of an exact solution process. The approximate solution process is one of generating a finite set of downwash sheets and constructing linear combinations of these sheets to satisfy the boundary conditions at a finite set of pre-selected control points on the surface.

The downwash sheets are obtained through an evaluation of the downwash integral using assumed pressure distributions that satisfy the required loading conditions on the planform edges.

The assumption usually made is that if the boundary conditions are satisfied at a suitable number of control points distributed over the surface then boundary conditions over the rest of the surface will be satisfied within small error limits.

This approximate procedure is equivalent to assuming that the downwash sheets may be represented by a series of polynomials that are continuous over the surface and may be combined to satisfy the surface boundary conditions at arbitrary control points.

This procedure provides reasonable results for analyses of configurations having continuous downwash distribution, however it may fail to produce consistently accurate results when applied to analyses of wing-control surface configurations that have discontinuous downwash distributions.

The direct solution process, described above, has been modified to provide a systematic procedure for obtaining accurate solutions of configurations having discontinuous downwash distributions and is described as follows:

Consider the downwash integral equation written in matrix form:

$$|W| = \left[\iint \Delta P \; K \, d\xi d\eta\right] |a| \tag{24}$$

where

$|W|$ is the kinematic downwash obtained from the known motion of the lifting surface and includes the factor $4\pi\rho V^2$ of equation (2).

$\left[\iint \Delta P \; K d\xi d\eta\right]$ a matrix of discrete values representing downwashes calculated at pre-selected collocation stations due to a set of assumed pressure distributions, ΔP .

$|a|$ is an array of pressure coefficients that are evaluated by applying a standard matrix inversion and multiplication procedure to equation (24).

Surface distributions of individual downwash sheets generated from an evaluation of the integral are generally quite smooth provided that the assumed pressure distribution ΔP is also smooth and does not contain singularities within regions interior of the planform edges. Figure 10 presents examples of chordwise downwash distributions obtained for the midspan station of a rectangular wing in steady flow. The pressure distributions used in the integral evaluation are composed of chordwise distributions shown on the left hand side of figure 10 coupled with a single sine wave in the spanwise direction. The surface distributions of the first four downwash sheets are smooth and continuous and may be accurately represented by polynomial expressions.

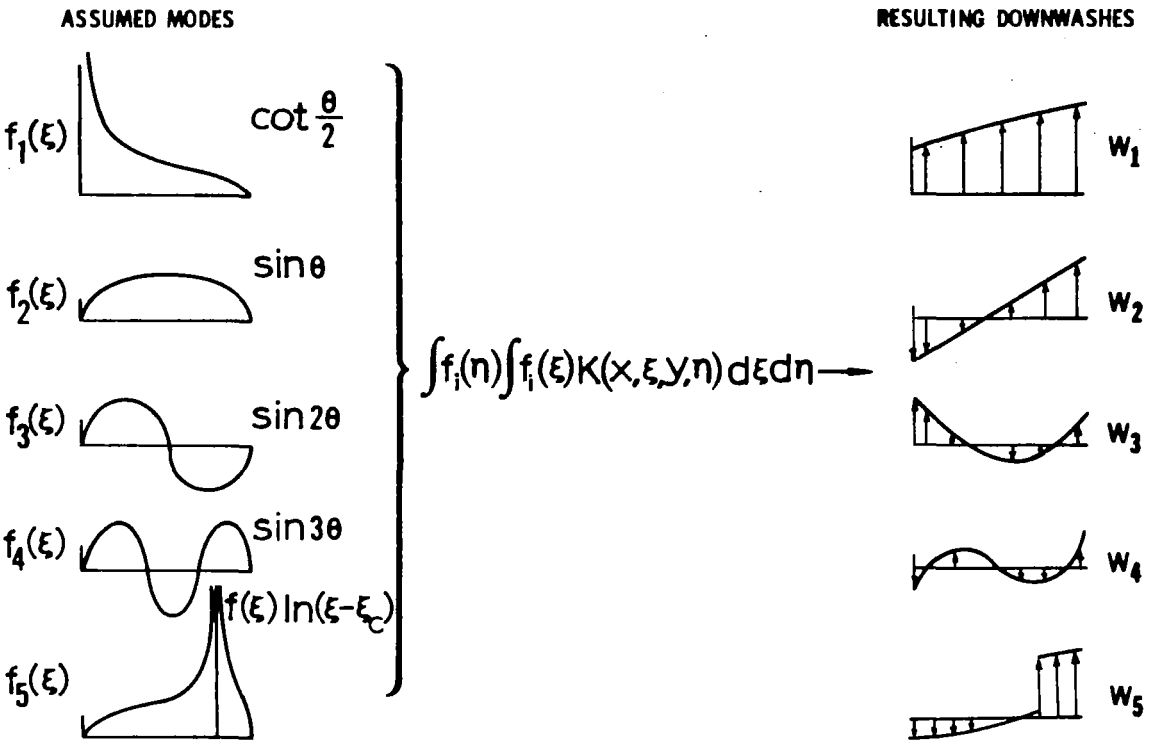

Figure 10.- Chordwise Downwash Distribution Resulting from the Integral Evaluation Using Assumed Pressure Distributions

An example of applying the direct solution process to configurations having continuous downwash distribution is shown in figure 11. The solution is formulated by constructing a linear combination of continuous downwash sheets to match the kinematic downwash distribution at a set of pre-selected control stations located on the surface. This linear combination of continuous downwash distributions usually provides a reasonable approximation of the kinematic distribution such that the integrated value of least-squares error in downwash over the surface would be very small.

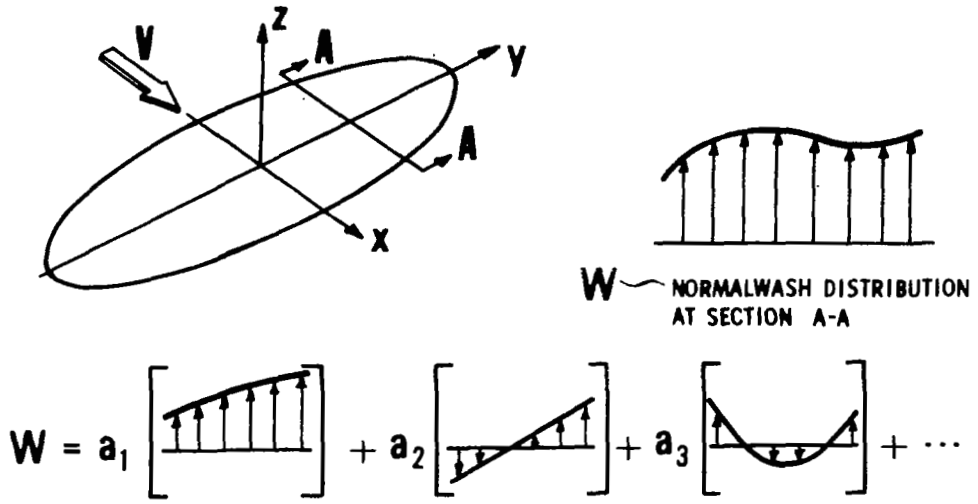

Figure 11.- Direct Solution Process Applied to Continuous Downwash Distributions

Although the direct solution process will provide accurate results for continuous lifting surface configurations, it may fail to provide consistently accurate results for configurations having discontinuous downwash distributions such as wing-control surface combination. Discontinuous downwash distributions such as a step function change in downwash across the control surface hingeline can be represented by a series of polynomials only in an approximate sense, as indicated by the solution process given in figure 12.

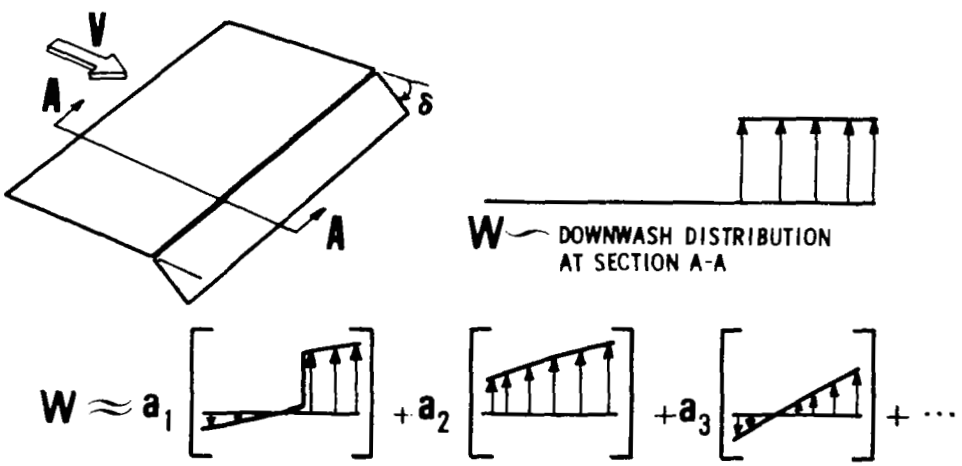

Figure 12.- Approximate Solution Process Applied to Configurations having Discontinuous Downwash Distributions

The resulting mathematical downwash distribution obtained from a summation of individual downwash sheets, shown in figure 12, would exactly satisfy the kinematic distribution at the selected control stations, however the distribution between the control stations may deviate grossly from the kinematic distribution and produce large values of least-squares error in downwash over the surface. The solution would also be very sensitive to the number of downwash sheets used in the approximation as well as being sensitive to the relative locations of the control points distributed over the surface.

A more systematic solution process applied to the solution of planforms having discontinuous downwash distributions is one of developing a mathematical downwash distribution that has identical discontinuity values that are contained in the kinematic distribution and subtracting this distribution from the original, thus providing a downwash distribution that is continuous over the surface for which the direct lifting surface solution process may be readily applied.

This preferred solution process for discontinuous downwash distributions is given by the matrix equation

$$\left|W(x,y)\right| - \left[\iint \Delta P_s K(\xi,\eta)\,d\xi\,d\eta\right] a_k \longrightarrow \left|\bar{W}_{mod}(x,y)\right|$$

$$\left|\bar{W}_{mod}(x,y)\right| = \left[\iint \Delta P_r K(\xi,\eta)\,d\xi\,d\eta\right] \left|\, a \,\right| \qquad (25)$$

where $\bar{W}_{mod}(x,y)$ is the continuous downwash distribution obtained by subtracting from the kinematic distribution a distribution having identical values of discontinuities that are contained in the kinematic distribution.

ΔP_s the singular pressure distributions that provide the same discontinuity characteristics contained in the kinematic downwash distribution.

ΔP_r the regular pressure distributions used to define continuous downwash distributions.

A graphic display of the preferred solution process is shown in figure 13.

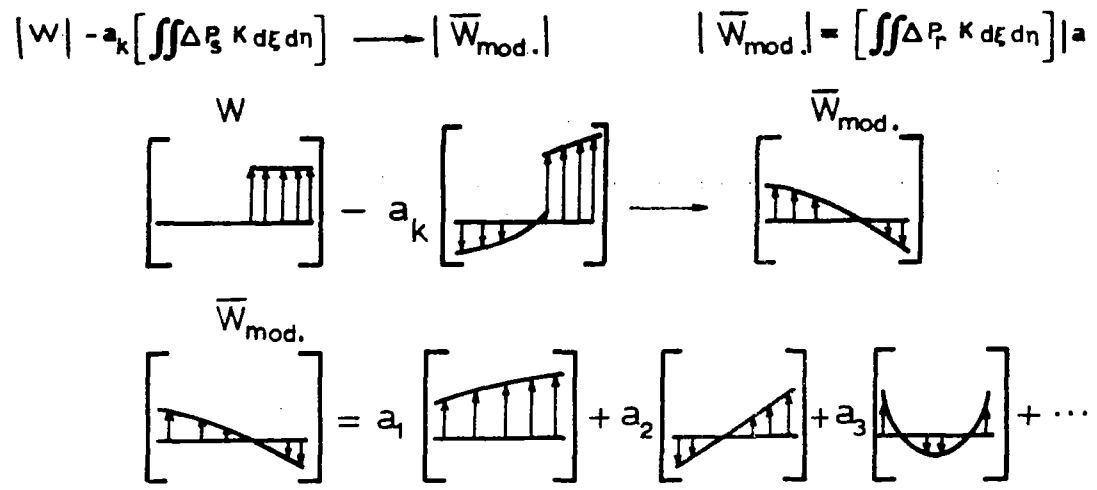

Figure 13.- Systematic Solution Process Suggested for use on Configurations having Discontinuous Downwash Distributions

The pressure distribution resulting from the solution process is the sum of the pressures that provide the discontinuity characteristics and the regular pressure distributions obtained as a solution of modified downwash distribution $\overline{W}_{mod}(x,y)$.

The key to this solution process is the development of pressure distributions having known strengths that provide identical values of downwash discontinuities contained in the kinematic distribution. Formulation of the analytical pressure expressions that provide the required discontinuities in boundary conditions have been well documented by Landahl (reference 3) and Ashley (reference 10) and are briefly discussed in the following section.

Pressure Distributions

Use of the preferred solution process requires two pressure distributions to be defined over the lifting surface planform. One of the distributions to provide identical value of downwash discontinuity characteristics as defined by the kinematic downwash distribution and the second pressure function to provide smooth and continuous downwash distributions over the surface.

Pressure distributions having known strengths that provide identical discontinuity values of downwash across the boundaries of the control surface have been developed by Landahl (reference 3) for the inboard partial span control surface case and by Ashley (reference 10) for the case of a control surface that extends to the planform side edge.

The linearized lifting surface problem presented in reference 3 has been formulated using nondimensional variables throughout its derivation. The cartesian coordinates (x,y,z) are nondimensionalized with respect to the reference length b_0, the root semichord. Also, time is nondimensionalized and is defined as

$$t = \frac{V_\infty}{b_0}\tau$$

where V_∞ is the free-stream velocity

b_0 is the root semichord

τ is time

The equations of motion given by equation (1) are then revised in terms of the pressure perturbation $c_p = \mathrm{Re}\left[\bar{P} \cdot \exp(ikt)\right]$ to provide the following equation that is satisfied by the linearized approximation $\bar{P}$.

$$(1-M^2)\,\bar{P}_{\xi\xi} + \bar{P}_{\eta\eta} + \bar{P}_{\zeta\zeta} - 2ikM^2\bar{P}_{\xi} + k^2M^2\bar{P} = 0 \qquad (26)$$

where $\bar{P}$ is defined as

$$\bar{P} = \frac{P-P_\infty}{\rho V^2/2}$$

The boundary condition to be satisfied off of the lifting surface is $\bar{P}(\xi,\eta,0) = 0$ and using the condition of normalwash on the wing along with the relationship of pressure perturbation to velocity perturbation potential the boundary condition to be satisfied on the wing is given as:

$$\bar{P}_{\zeta} = -2\left[\frac{\partial^2\bar{H}(\xi,\eta)}{\partial\xi^2} + 2ik\,\frac{\partial\bar{H}(\xi,\eta)}{\partial\xi} - k^2\,\bar{H}(\xi,\eta)\right] \qquad (27)$$

where $\bar{H}(\xi,\eta)$ is the deflection shape defined by $\bar{H}(\xi,\eta) = H(\xi,\eta)/b_0$

The definition of the lifting surface deflection due to a trailing edge control surface oscillation about a hinge line is given as:

$$\bar{H}(\xi,\eta) = \Theta(\eta) \cdot (\xi-x_c) \cdot U(\xi-x_c) \cdot U(\eta-y_i) \qquad (28)$$

where $\Theta(\eta)$ is the angular rotation of the control surface at η measured in a plane perpendicular to the y axis.

x_c is the hingeline coordinate

y_i is the side edge coordinate

$U(\xi-x_c)$ is a unit function of $(\xi-x_c)$

$U(\eta-y_i)$ is a unit function of $(\eta-y_i)$

Inserting equation (28) into equation (27) and performing the indicated differentiations results in the following boundary conditions that are to be satisfied by the pressure function.

$$\bar{P}_\zeta = \begin{cases} -2\theta(\eta)\left[\delta(\xi-x_c) + 2ik - k^2(\xi-x_c)\right]U(\eta-y_i) & \xi \geqslant x_c \\ & \eta \geqslant y_i \\ 0 & \xi < x_c \end{cases} \tag{29}$$

where $\delta(\xi-x_c)$ is the Dirac delta function

The method of asymptotic expansions is applied to determine the behavior of the pressure distribution, in the immediate vicinity of the control surface leading edge $\xi = x_c$ and at a side edge $\eta = y_i$. The effect of using the asymptotic expansions is to magnify the singular region by stretching the coordinates by a small quantity ε. Coordinate stretching has the effect of making the highest derivatives dominate in the singular region and allows the problem to be reduced to a solution of a much simpler problem in the immediate region of the singularity.

To determine the pressure distribution near the forward corner of a rectangular control surface all three independent variables are stretched in the following manner of

$$\bar{\xi} = \frac{(\xi-x_c)}{\varepsilon} \; ; \quad \bar{\eta} = \frac{(\eta-y_i)}{\varepsilon} \; ; \quad \bar{\zeta} = \frac{\zeta}{\varepsilon} \tag{30}$$

Also, $\bar{P}$ is represented by a series in ascending powers of ε given as

$$\bar{P} = \sum_n \bar{P}^{(n)} \varepsilon^n \tag{31}$$

Insertion of equation (30) and equation (31) into the differential equation and boundary conditions provides the boundary value problem given as:

$$\beta^2 \bar{P}_{\bar{\xi}\bar{\xi}} + \bar{P}_{\bar{\eta}\bar{\eta}} + \bar{P}_{\bar{\zeta}\bar{\zeta}} = 0$$

$$\bar{P}_{\bar{\zeta}}(\bar{\xi},\bar{\eta},0) = \begin{cases} -2\Theta(\eta)\left[\delta(\bar{\xi}) + 2ik\epsilon - k^2\epsilon^2\bar{\xi}\right] & \bar{\xi} \geq 0 \\ 0 & \bar{\xi} < 0 \end{cases} \qquad (31\text{-A})$$

Source distributions, that satisfy the differential equation, are selected on the basis of matching the boundary condition and results in a solution that correctly describes the pressure variation both near the control surface leading edge as well as near the corner of a non-swept control surface given as:

$$\bar{P}(\xi,\eta,0) = \frac{-\Theta(\eta)}{\pi\beta}\left[1 + 2ik(\xi-x_c)\right]\ln\left|\sqrt{(\xi-x_c)^2 + \beta^2(\eta-y_i)^2} - \beta(\eta-y_i)\right|$$

$$\frac{-\Theta(\eta)}{\pi}\left[2ik - k^2(\xi-x_c)\right](\eta-y_i)\ln\left|\sqrt{(\xi-x_c)^2 + \beta^2(\eta-y_i)^2} - (\xi-x_c)\right| \qquad (32)$$

Equation (32) may be modified to include hingeline sweep effects by multiplying the first term of equation (32) by $\beta/\beta_{h\ell}$.

$\beta_{h\ell}$ is defined as

$$\beta_{h\ell} = \sqrt{\beta^2 + \tan^2\Lambda_c} \qquad (33)$$

Λ_c is the sweep angle of the hingeline (positive when swept aft). Also, $\Theta(\eta)$ is understood to be the rotation angle of the control surface measured in a plane perpendicular to the y axis. The derived pressure distribution contains the expected logarithmic singularity along the hingeline. Landahl demonstrated that the solution also leads to a slope singularity in the spanwise loading across the side edge. It should be observed that the present derivation is not valid close to the rear corner of the control surface. Here the problem is complicated by mixed boundary values that must be considered as part of the "inner region". A solution was obtained in reference 11 by a method of images to meet the boundary condition at a rear corner of the control surface. It does not appear to be valid for a swept trailing edge however, and for this reason it has not been applied in the present program. Instead it was considered sufficient to extend Landahl's solution to the rear corner in the same manner as suggested in reference 3 .

Pressure distributions have been formulated in a similar manner by Ashley (reference 10) for the control surface that extends to the tip of the planform. The boundary value problem differs from those treated by Landahl in that a mixed flow boundary condition must be accounted for in the solution.

Following the derivation of reference 3 the first order "inner problem" is defined at the hingeline of the control surface side edge as:

$$\bar{C}_{P_{\bar{\eta}\bar{\eta}}} + \bar{C}_{P_{\bar{\xi}\bar{\xi}}} + \frac{\beta_n^2}{\cos^2\Lambda_c}\,\bar{C}_{P_{\bar{\xi}\bar{\xi}}} + 2\tan\Lambda_c \bar{C}_{P_{\bar{\xi}\bar{\eta}}} = 0 \tag{34}$$

$$\text{where } \bar{C}_p = \frac{P-P_\infty}{\rho V^2/2}\ ; \text{ and } \beta_n^2 = 1 - M^2\cos^2\Lambda_c$$

Boundary conditions of equation (34) are specified by:

$$\begin{aligned} \bar{C}_{p_{\bar{\zeta}}}(\bar{\xi},\bar{\eta},0) &= 2\Theta(\eta)\,\delta(\bar{\xi}) \qquad \bar{\eta} \geq 0 \\ \bar{C}_p(\bar{\xi},\bar{\eta},0) &= 0 \qquad\qquad\quad \bar{\eta} < 0 \end{aligned} \tag{35}$$

Solutions of equation (34) subject to the boundary conditions of equation (35), are obtained by reducing the equation to a much simpler form by applying a Fourier transformation on $\bar{\xi}$ and after considerable manipulations the first order solution is given as:

$$\begin{aligned} \bar{C}_p^{(0)}(\bar{\xi},\bar{\eta},0) = \frac{\Theta(\eta)}{\pi\left[\beta^2+\tan^2\Lambda_c\right]^{1/2}} \int_0^{\frac{\beta\bar{\eta}}{\bar{\xi}}} \left[q^2+\left(1-q\,\frac{\tan\Lambda_c}{\beta}\right)^2\right]^{-1/2} \cdot \\ \cdot \left\{ \left[\left(1+\frac{\tan^2\Lambda_c}{\beta^2}\right)^{1/2} - 1\right]^{1/2} \cdot \left[\left(1+\left(\frac{1}{q}-\frac{\tan\Lambda_c}{\beta}\right)^2\right)^{1/2} - 1\right]^{1/2} \right. \\ \left. - \left[\left(1+\frac{\tan^2\Lambda_c}{\beta^2}\right)^{1/2} + 1\right]^{1/2} \cdot \left[\left(1+\left(\frac{1}{q}-\frac{\tan\Lambda_c}{\beta}\right)^2\right)^{1/2} + 1\right]^{1/2} \right\} dq \end{aligned} \tag{36}$$

where

$$q = \frac{\beta\bar{\eta}_1}{\bar{\xi}}$$

The above integral may be reduced further to provide the following expression for $\bar{C}_p(\xi,\eta,0)$ at the control surface tip station.

$$\bar{C}_p^{(0)} = \frac{\Theta(\eta)}{\pi(\beta^2+\tan^2\Lambda_c)^{1/2}} \ln \left| \frac{\sqrt{\left[(\xi-x_c)^2+\beta^2(s-\eta)^2\right]^{1/2}+\beta(s-\eta)} - \sqrt{2\beta(s-\eta)}}{\sqrt{\left[(\xi-x_c)^2+\beta^2(s-\eta)^2\right]^{1/2}+\beta(s-\eta)} + \sqrt{2\beta(s-\eta)}} \right| \tag{37}$$

The distribution obtained by this solution process appears to be correct since $\bar{C}_p(\xi,\eta)$ approaches zero having an infinite slope proportional to the square root of the distance from the wing-tip and also contains a $\ln(\xi-x_c)^2$ term that provides the proper streamwise discontinuity in downwash across the hingeline.

Pressure distributions obtained by the above described asymptotic expansion process are valid only in localized regions of the planform since the distributions of the outer regions have not been defined nor matched with the inner region solutions. However, the essential part of the pressure distribution that provides the discontinuities in downwash along the control surface edges is defined by the inner region solution. The distribution in the outer regions may take on any convenient form that satisfies the required loading condition along the edges of the planform since a unique distribution is not being determined at this stage of the solution process. Consequently, the surface pressure loading functions that provide the downwash discontinuities are obtained by extending the applicable range of the inner solution and modifying these distributions to meet the condition of having the pressures vanish in proportion to the square root of the distance from the edges.

Pressure loading functions are developed to provide analysis capability for a vast array of control surface configurations. The most convenient manner to describe the loading distributions due to motions of multiple control surfaces is to describe the surface loadings for two particular configurations and form combinations of these to represent any desired configuration.

The two basic control surface configurations for which loading functions are developed are shown in figure 14 and figure 15.

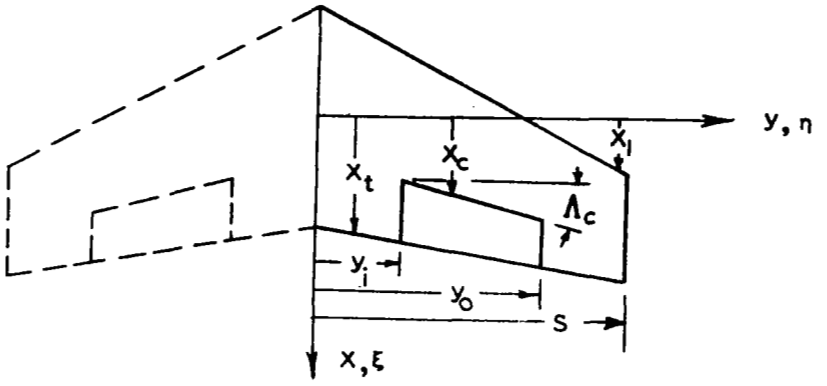

Figure 14.- Planform Definition Used to Describe Loading Functions for an Inboard Control Surface

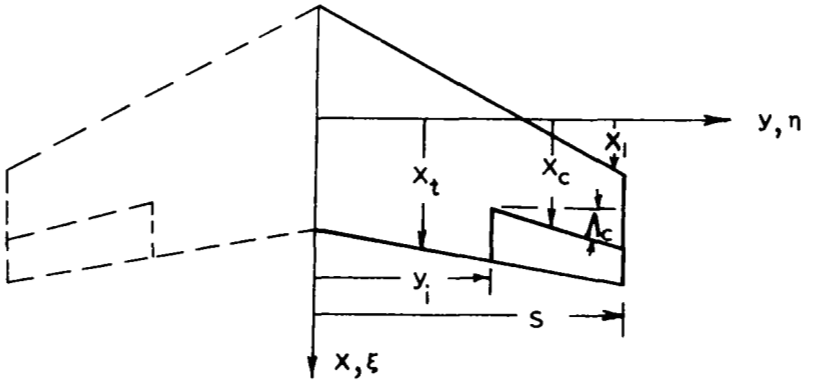

Figure 15.- Planform Definition Used to Describe Loading Functions for an Outboard Control Surface

The pressure loading functions are defined over the surface only in terms of the pressure loadings caused by motions of the right hand side control surface. For symmetrical control surface deflections, the pressure distributions over the lifting surface due to motions of the left hand side control surface are identical to that of the right hand side, but are reversed left to right, as in a mirror image. Consequently, the complete symmetrical or antisymmetrical loadings may be formulated using only the pressure expression due to motions of the right hand side control surface. This is accomplished for the symmetrical case by defining the total pressure existing at an (η) station to be the sum of the pressure at $(+\eta)$ and those at $(-\eta)$ within the pressure expression describing the loadings caused by motions of the right hand side control surface. The total antisymmetrical loadings at an (η) station are formulated by subtracting the loadings at $(-\eta)$ from those at $(+\eta)$ within the pressure expression defining loadings caused by motions of the right hand side control surface.

Loading functions for the inboard partial-span control surface. --- The pressure loading functions formulated for an inboard partial-span control surface in terms of the geometrical properties of the right hand side are given in the expression:

$$\Delta P_s(\xi,\eta) = 4\rho V^2(s^2-\eta^2)^{1/2}\, f_s(\eta)\, g_s(\xi,\eta) \tag{38}$$

where

$$f_s(\eta) = \Theta(\eta)/4\pi(\beta^2 + \tan^2\Lambda_c)^{1/2}(s^2-\eta^2)^{1/2} \tag{38a}$$

$$g_s(\xi,\eta) = -g_1(\eta) + k^2(\xi-x_c)g_2(\eta) - 2ik\,(\xi-x_c)g_1(\eta)+g_2(\eta) \tag{39}$$

$\Theta(\eta)$ is the rotation angle at the hingeline measured in a plane perpendicular to the y axis.

Λ_c is the sweep angle of the hingeline (positive swept back)

Subscript s denotes that the pressure distributions contain singularities. The $g_1(\eta)$ and $g_2(\eta)$ terms in equation (39) are control functions to provide either symmetrical or antisymmetrical loadings and are defined as:

$$g_1(\eta) = g_1^R(\eta) + S_F\, g_1^R(-\eta)$$

$$g_2(\eta) = g_2^R(\eta) + S_F\, g_2^R(-\eta) \tag{40}$$

S_F is a sign factor that takes on values of $S_F = +1.0$ for symmetrical loadings and $S_F = -1.0$ for antisymmetrical loadings.

The $g_1^R(\eta)$ and $g_2^R(\eta)$ functions are non-singular in regions outside of the control surface boundaries for values of $\eta < y_i$ and $\eta > y_o$ The singularity is turned on at $\eta = y_o$ and its strength is maintained over the spanwise length of the hingeline up to $\eta = y_i$, where the singularity is turned off. For stations inboard of $\eta = y_i$ the functions are non-singular and are extended to the left hand tip of the planform.

$$g_1^R(\eta) = e_1(\xi)\cdot h(\eta)\left[\ln \left| \left[(\xi-x_c)^2+\beta^2(y_o-\eta)^2\right]^{1/2}-\beta(y_o-\eta)\right| \right.$$
$$\left. - \ln \left| \left[(\xi-x_c)^2+\beta^2(y_i-\eta)^2\right]^{1/2}-\beta(y_i-\eta)\right| \right] \qquad (41)$$

$$g_2^R(\eta) = (\beta^2 + \tan^2 \Lambda_c)^{1/2}\, h(\eta)\cdot$$
$$\cdot \left\{ e_2(\xi,\eta,y_o)(y_o-\eta)\left[\ln \left| \left[(\xi-x_c)^2+\beta^2(y_o-\eta)^2\right]^{1/2}-(\xi-x_c)\right| \right.\right.$$
$$\left. - \ln \left| \left[(x_\ell-x_c)^2+\beta^2(y_o-\eta)^2\right]^{1/2}-x_\ell-x_c)\right| \right]$$
$$- e_2(\xi,\eta,y_i)(y_i-\eta)\left[\ln \left| \left[(\xi-x_c)^2+\beta^2(y_i-\eta)^2\right]^{1/2}-(\xi-x_c)\right| \right.$$
$$\left.\left. -\ln \left| \left[(x_\ell-x_c)^2+\beta^2(y_i-\eta)^2\right]^{1/2}-(x_\ell-x_c)\right| \right] \right\} \qquad (42)$$

The $e_1(\xi)$ factor on $g_1^R(\eta)$ modifies the chordwise pressure function such that the pressure vanishes at the leading and trailing edge in a square root manner and maintains the required strength at the hingeline to provide the discontinuities across the hingeline.

$$e_1(\xi) = \left[\frac{(x_t-\xi)(\xi-x_\ell)}{(x_t-x_c)(x_c-x_\ell)}\right]^{1/2} \left[1 - \frac{1}{2}(\xi-x_c)\left(\frac{1}{x_c-x_\ell} - \frac{1}{x_\ell-x_c}\right)\right] \qquad (43)$$

The $e_2(\xi,\eta,y_s)$ factor contained in $g_2^R(\eta)$ forces the pressures to vanish having an infinite slope everywhere along the trailing edge except at the control surface side edge where the singularity strengths are maintained to provide the proper change in boundary condition across the side edge. Using y_s to represent y_i or y_o

$$e_2(\xi,\eta,y_s) = \left[\frac{(x_c-\xi)^2}{(x_t-\xi)^2 + \beta^2(y_s-\eta)^2}\right]^{1/4} \qquad (44)$$

The $h(\eta)$ function is used to force the pressures to zero at the planform side edges while maintaining second derivative continuity in the spanwise loading.

$$h(\eta) = \begin{cases} \left[\dfrac{(s-y_s)^2 - (y_s-\eta)^2}{(s-y_s)^2}\right]^{1/2}\left[1 + \dfrac{1}{2}\dfrac{(y_s-\eta)^2}{(s-y_s)^2}\right] & y_s \leq \eta \leq s \\ 1.0 & -y_s < \eta < y_s \\ \left[\dfrac{(s-y_x)^2 - (y_s+\eta)^2}{(s-y_s)^2}\right]^{1/2}\left[1 + \dfrac{1}{2}\dfrac{(y_s+\eta)^2}{(s-y_s)^2}\right] & -s \leq \eta \leq -y_s \end{cases} \quad (45)$$

Loading functions for outboard partial-span control surfaces. -- The pressure loading functions for configurations having a control surface side edge at the planform side edge typical of configurations shown in Figure 15 are formulated in the following manner:

$$\Delta P_s(\xi,\eta) = 4\rho V^2 (s^2-\eta^2)^{1/2} f_s(\eta) \; g_s(\xi,\eta) \quad (46)$$

having functions similar to the inboard control surface pressure definitions given by

$$f_s(\eta) = \Theta(\eta)/4\pi(\beta^2+\tan^2\Lambda)^{1/2} (s^2-\eta^2)^{1/2}$$

$$g_s(\xi,\eta) = -g_1(\eta) + k^2(\xi-x_c)\, g_2(\eta) - 2ik\left[(\xi-x_c)\, g_1(\eta) + g_2(\eta)\right] \quad (47)$$

The $g_1(\eta)$ and $g_2(\eta)$ functions provide symmetric or antisymmetric analysis capability and are defined as:

$$g_1(\eta) = g_1^R(\eta) + S_F\, g_1^R(-\eta)$$

$$g_2(\eta) = g_2^R(\eta) + S_F\, g_2^R(-\eta) \quad (48)$$

where $S_F = 1.0$ for symmetric analyses

$S_F = -1.0$ for antisymmetric analyses.

The $g_1^R(\eta)$ and $g_2^R(\eta)$ functions turn on the singularity at the planform side edge and turn it off at the inboard side edge of the control surface at $\eta = y_i$.

$$g_1^R(\eta) = e_1(\xi)\, h_\ell(\eta) \cdot \left\{ \ln \left| \frac{\sqrt{\left[(\xi-x_c)^2+\beta^2(s-\eta)^2\right]^{1/2}+\beta(s-\eta)} - \sqrt{2\beta(s-\eta)}}{\sqrt{\left[(\xi-x_c)^2+\beta^2(s-\eta)^2\right]^{1/2}+\beta(s-\eta)} + \sqrt{2\beta(s-\eta)}} \right| \right.$$

$$\left. - h_r(\eta) \ln \left| \left[(\xi-x_c)^2+\beta^2(y_i-\eta)^2\right]^{1/2} - \beta(y_i-\eta) \right| \right\} \tag{49}$$

$$g_2^R(\eta) = (\beta^2 + \tan^2 \Lambda_c)^{1/2}\, h_\ell(\eta) \cdot \left\{ (s-\eta) e_3(\xi,\eta,s) \left[\ln \left| \left[(\xi-x_c)^2+\beta^2(s-\eta)^2\right]^{1/2} - (\xi-x_c) \right| \right.\right.$$

$$\left. - \ln \left| \left[(x_\ell-x_c)^2+\beta^2(s-\eta)^2\right]^{1/2} - (x_\ell-x_c) \right| \right]$$

$$- h_r(\eta)(y_i-\eta) e_2(\xi,\eta,y_i) \left[\ln \left| \left[(\xi-x_c)^2+\beta^2(y_i-\eta)^2\right]^{1/2} - (\xi-x_c) \right| \right.$$

$$\left.\left. - \ln \left| \left[(x_\ell-x_c)^2+\beta^2(y_i-\eta)^2\right]^{1/2} - (x_\ell-x_c) \right| \right] \right\} \tag{50}$$

where $e_1(\xi)$ is defined by equation (43)

$e_2(\xi,\eta,y_i)$ is defined by equation (44)

The modifying side edge function $e_3(\xi,\eta,s)$ maintains the proper singularity strength at the side edge and forces the pressure to vanish at the trailing edge with an infinite slope.

$$e_3(\xi,\eta,s) = \left[\frac{x_t-\xi}{(x_t-\xi) + \beta(s-\eta)} \right]^{1/2} \tag{51}$$

The $h_\ell(\eta)$ and $h_r(\eta)$ are the modifying functions that satisfy the planform edge boundary condition while maintaining a second derivative continuity in spanwise loadings and are defined as:

$$h_\ell(\eta) = \begin{cases} 1.0 & \eta \geq -y_i \\ \left[\dfrac{(s-y_i)^2-(y_i+\eta)^2}{(s-y_i)^2} \right]^{1/2} \left[1+\dfrac{1}{2} \dfrac{(y_i-\eta)^2}{(s-y_i)^2} \right] & \eta < -y_i \end{cases} \tag{52}$$

$$h_r(\eta) = \begin{cases} \left[\dfrac{(s-y_i)^2-(y_i-\eta)^2}{(s-y_i)^2}\right]^{1/2} \left[\, 1+\dfrac{1}{2}\ \dfrac{(y_i-\eta)^2}{(s-y_i)^2}\,\right] & \eta \geq y_i \\ 1.0 & \eta < y_i \end{cases} \tag{53}$$

Insertion of the above pressure expressions into the downwash integral provides mathematical downwash sheets having identical discontinuity distributions as contained in the kinematic distribution. Subtraction of these downwash sheets from the kinematic distribution results in a modified downwash distribution for which direct solutions may be obtained using a regular lifting surface pressure distribution defined by:

$$\Delta P_r(\xi,\eta) = 4\rho V^2\ (s^2-\eta^2)^{1/2} \sum_m \sum_n a_{nm} f_r^{(n)}(\eta) \cdot g_r^{(m)}(\xi,\eta) \tag{54}$$

where

a_{nm} are the unknown coefficient multipliers

$$f_r^{(n)}(\eta) = \frac{\sin(n\Phi)}{\sin\Phi} \qquad n = \begin{matrix} 1,3,5....\text{symmetrical} \\ 2,4,6....\text{antisymmetrical} \end{matrix} \tag{55}$$

$$\Phi = \cos^{-1}(\eta/s)$$

$$g_r^{(m)}(\xi,\eta) = \begin{cases} \cot\dfrac{\Theta}{2} & m = 1 \\ \sin(m-1)\Theta & m = 2,3,4,... \end{cases} \tag{56}$$

where the chordwise angular coordinate is defined as:

$$\Theta = \cos^{-1}\left[-\left(\frac{\xi-x_m(\eta)}{b(\eta)}\right)\right] \qquad x_m(\eta) = \frac{x_t(\eta) + x_\ell(\eta)}{2}$$

The chordwise angular coordinate Θ is not to be confused with the control surface rotation angle $\theta(\eta)$.

Final Form of the Downwash Integral Equation

The final expression of the downwash-pressure integral equation is formulated using the preferred solution process previously described for evaluating the loadings on lifting surfaces having discontinuous downwash distributions.

The matrix form of the equation is given as:

$$4\pi\rho V^2\left[\frac{\partial H(x,y)}{b_o\partial x} + ik\frac{H(x,y)}{b_o}\right] - \left[\iint \Delta P_s(\xi,\eta)K(x,\xi,y,\eta)d\xi d\eta\right]$$

$$= \left[\iint \Delta P_r(\xi,\eta)K(x,\xi,y,\eta)d\xi d\eta\right]\left|a_{nm}\right| \qquad (57)$$

The form of equation (57) is slightly different from that given by equation (25) in that the coefficient $a_k(\eta)$ is placed inside of the integral as a multiplier on $\Theta(\eta)$ rather than being used as a constant multiplier outside of the integral. $a_k(\eta)$ represents a polynomial defining the spanwise twist distribution of the control surface and allows calculation of a variable downwash discontinuity along the hingeline.

The first matrix on the left hand side represents an array of values defining the kinematic downwash at pre-selected collocation stations distributed over the surface. The second matrix represents an array of downwashes evaluated at the same stations using a known pressure distribution that provides the same discontinuities that are contained in the kinematic distribution.

The calculated downwash distribution is subtracted from the kinematic distribution to form a modified distribution that is smooth and continuous. Integral equation solutions using the modified distribution as new boundary conditions are obtained by the direct assumed mode solution process.

The spanwise integral on the left hand side of equation (57) is evaluated using logarithmic quadratures in the vicinity of the downwash chord to evalute the spanwise singularity that has been previously identified. The singularities are removed from the integral on the right hand side of equation (57) and evaluated individually since a meaningful Taylor series expansion may be made for the continuous pressure distributions used in the direct solution process.

The expression defining the mathematical discontinuous downwash distribution represented by the second term on the left hand side of equation (57) is given by the following:

$$\int_{-s}^{s}\int_{x_\ell}^{x_t} \Delta P_s(\xi,\eta)K(x,\xi,y,\eta)d\xi\,d\eta = \int_{-s}^{s} (s^2-\eta^2)^{1/2}\, f_s(\eta)\left\{ C_s(y,\eta) + C_{ns}(y,\eta) + \frac{f_s(y)}{f_s(\eta)}\left[\frac{C_1^s(y,y)}{(y-\eta)^2} - \frac{s^2-y^2}{s^2-\eta^2}\,\frac{D_1^s(x,y)}{y-\eta}\right]\right\} d\eta + \pi f_s(y) C_1^s(y,y) \tag{58}$$

where $C_s(y,\eta)$ and $C_{ns}(y,\eta)$ represent the chordwise integrals due to the singular and non-singular parts of the kernel function and are given as:

$$C_s(y,\eta) = \int_{x_\ell}^{x_t} g_s(\xi,\eta)e^{ik(x-\xi)}\left\{ -\frac{1}{(y-\eta)^2}\left[1 + \frac{x-\xi}{\left[(x-\xi)^2+\beta^2(y-\eta)^2\right]^{1/2}}\right] + \frac{ik}{\left[(x-\xi)^2+\beta^2(y-\eta)^2\right]^{1/2}} - \frac{k^2}{2}\ln\left|\left[(x-\xi)^2+\beta^2(y-\eta)^2\right]^{1/2} - (x-\xi)\right| - \frac{k^2}{2\beta^2}\left[\frac{x-\xi}{\left[(x-\xi)^2+\beta^2(y-\eta)^2\right]^{1/2}} - M\right]\right\} d\xi \tag{59}$$

$$C_{ns}(y,\eta) = \int_{x_\ell}^{x_t} g_s(\xi,\eta)\, K_{ns}(x-\xi,y-\eta)d\xi \tag{60}$$

where $g_s(\xi,\eta)$ is the pressure function defined by either equation (39) or equation (47).

$h(\eta)$ is the spanwise pressure modifying function defined either by equation (45) or by equation (52) depending upon the configuration being evaluated.

The $C_1^s(y,y)$ and $D_1^s(y,y)$ terms are due to the Hsu integration process where the chordwise integral at $\eta = y$ and the spanwise derivative are removed from the integrand and are defined as:

$$C_1^s(y,y) = 2\int_{x_\ell}^{x} g_s(\xi,\eta)\, e^{-ik(x-\xi)}\, d\xi \tag{61}$$

$$D_1^s(x,y) = \frac{f_s'(\eta)_{\eta=y}}{f_s(y)} C_1^s(y,y) + C_2^s(y,y) + r^s(x,y) \tag{62}$$

$$C_2^s(y,y) = 2 \int_{x_\ell}^{x} k_s(\xi,y)\, e^{-ik(x-\xi)}\, d\xi \tag{63}$$

$$k_s(\xi,y) = \begin{cases} \frac{\partial}{\partial \eta}\left[g_s(\xi,\eta)\right]_{\eta=y} + e^{-ik(\xi-x_c)} \cdot \frac{2\tan\Lambda_c}{(\xi-x_c)} & y_i < \eta < y_o \\ \frac{\partial}{\partial \eta}\left[g_s(\xi,\eta)\right]_{\eta=y} & \eta \leq y_i \text{ and } \eta \geq y_o \end{cases} \tag{64}$$

$$r^s(x,y) = \begin{cases} 0 & \eta \leq y_i \text{ and } \eta \geq y_o \\ -e^{-ik(x-x_c)}\, 4\tan\Lambda_c \ln\left| \frac{x-x_c}{x_\ell - x_c} \right| & y_i < \eta < y_o \end{cases} \tag{65}$$

The mathematical continuous downwash distributions represented by the last term of equation (57) are evaluated by removing the spanwise singularity from the integrand to produce an integrand that is smooth and continuous and easily evaluated by a few spanwise quadrature terms. The singularities are identified by developing a Taylor series expansion of $\Delta P_r(\xi,\eta)\, e^{-ik(x-\xi)}$, and performing the chordwise integration as indicated in a previous section.

The expression defining the mathematical continuous downwash distributions represented by the last term of equation (57) is given as:

$$\int_{-s}^{s} \int_{x_\ell}^{x_t} \Delta P_r(\xi,\eta) K(x-\xi, y-\eta)\, d\xi\, d\eta = \int_{-s}^{s} \left(s^2-\eta^2\right)^{1/2} f_r(\eta) \left\{ C_s^r(y,\eta) + C_{ns}^r(y,\eta) + \frac{f_r(y)}{f_r(\eta)} \left[\frac{C_1^r(y,y)}{(y-\eta)^2} - \frac{D_1^r(x,y)}{y-\eta} - \left[D_2(x,y) + (y-\eta)\, D_3(x,y) \right] \ln\beta^2 (y-\eta)^2 \right] \right\} d\eta$$

$$+ \pi f_r(y) \left\{ C_1^r(y,y) + y D_1^r(x,y) + D_2(x,y) \left[y^2 + s^2 \left(\ln\left| \frac{\beta s}{2} \right| - \frac{1}{2} \right) \right] + D_3(x,y) \left[\frac{1}{3} y^3 + y s^2 \left(\ln\left| \frac{\beta s}{2} \right| - \frac{1}{2} \right) + y s^2 \right] \right\} \tag{66}$$

The subscript r denotes that smooth and continuous pressure distributions defined by equation (55) and equation (56) are being used in this integral evaluation.

$C_s^r(y,\eta)$ and $C_{ns}^r(y,\eta)$ represent the chordwise integrals due to the singular and non-singular parts of the kernel function.

$$C_s^r(y,\eta) = \int_{x_\ell}^{x_t} g_r(\xi,\eta)e^{-ik(x-\xi)} \left\{ -\frac{1}{(y-\eta)^2}\left[1 + \frac{x-\xi}{\left[(x-\xi)^2+\beta^2(y-\eta)^2\right]^{1/2}}\right] \right.$$

$$+ \frac{ik}{\left[(x-\xi)^2+\beta^2(y-\eta)^2\right]^{1/2}} - \frac{k^2}{2} \ln\left|\left[(x-\xi)^2+\beta^2(y-\eta)^2\right]^{1/2} - (x-\xi)\right|$$

$$\left. - \frac{k^2}{2\beta^2}\left[\frac{x-\xi}{\left[(x-\xi)^2+\beta^2(y-\eta)^2\right]^{1/2}} - M\right]\right\} d\xi \quad (67)$$

$$C_{ns}^r(y,\eta) = \int_{x_\ell}^{x_t} g_r(\xi,\eta)\, K_{ns}(x-\xi,y-\eta)\, d\xi \quad (68)$$

where $g_r(\xi,\eta)$ are the regular lifting surface pressure distributions of equation (56).

The $C_1^r(y,y)$ and $D_1^r(x,y)$ terms are due to the Hsu singularity subtraction process and defined as:

$$C_1^r(y,y) = 2\int_{x_\ell}^{x} g_r(\xi,\eta)\, e^{-ik(x-\xi)}\, d\xi \quad (69)$$

$$D_1^r(x,y) = \frac{f_s'(\eta)_{\eta=y}}{f_s(\eta)} C_1^r(y,y) + C_2^r(y,y) + r_r(x,y) \quad (70)$$

where

$$C_2^r(y,y) = 2\int_{x_\ell}^{x} k_r(\xi,y)\, e^{-ik(x-\xi)}\, d\xi \quad (71)$$

$$k_r(\xi,y) = \begin{cases} \frac{\partial}{\partial\eta}\left[g_r(\xi,\eta)\right]_{\eta=y} - \frac{e^{-ik(\xi-x_\ell)}}{2}\,\frac{\partial x_\ell}{\partial\eta}\,\frac{(x_t-\xi)^{1/2}}{(\xi-x_\ell)^{3/2}} & m = 1 \\ \frac{\partial}{\partial\eta}\left[g_r(\xi,\eta)\right]_{\eta=y} & m > 1 \end{cases} \tag{72}$$

$$r_r(x,y) = \begin{cases} -e^{-ik(x-x_\ell)}\,\frac{\partial x_\ell}{\partial\eta}\left[\frac{\pi}{2} + \arcsin\left(\frac{2x-(x_t+x_\ell)}{2b(y)}\right) + 2\left(\frac{x_t-x}{x-x_\ell}\right)^{1/2}\right] & m=1 \\ 0 & m>1 \end{cases} \tag{73}$$

The $D_2(x,y)$ and $D_3(x,y)$ terms are due to subtracting the spanwise logarithmic singularities from the integrand and are defined as:

$$D_2(x,y) = \frac{\beta^2}{2}\,\frac{\partial}{\partial\xi}\left[\, g_r(\xi,y)e^{-ik(x-\xi)}\right]_{\xi=x} - ikg_r(x,y) - \frac{k^2}{4}\,C_1^r(y,y) \tag{74}$$

$$D_3(x,y) = -\frac{\beta^2}{2}\,\frac{\partial^2}{\partial\xi\partial\eta}\left[\, g_r(\xi,\eta)e^{-ik(x-\xi)}\right]_{\substack{\xi=x \\ \eta=y}} + ik\,\frac{\partial}{\partial\eta}\left[g_r(x,\eta)\right]_{\eta=y} + \frac{k^2}{4}\left[C_2^r(y,y) + r^r(x,y)\right] \tag{75}$$

Numerical evaluation of the above downwash integrals is accomplished by subdividing the integration intervals into small regions and applying integration quadrature formulas appropriate to the function characteristics. Gaussian quadrature formulas containing unity, square-root, and logarithmic weight functions have been extensively used in the integral evaluations and are annotated throughout the computer program listing (reference 4) and need not be discussed here.

Generalized Forces

Generalized forces are formulated using two sets of pressure distributions that result from the modified solution process and are given in the following form applicable to the half-span wing;

$$Q_{ij} = \int_0^{b_o s} \int_{b_o x_\ell}^{b_o x_t} \Delta P_j(\xi,\eta)\, H_i(\xi,\eta)\, d(b_o\xi)\, d(b_o\eta) \qquad (76)$$

where $H_i(\xi,\eta)$ is the i^{th} deflection mode shape.

$\Delta P_j(\xi,\eta)$ is the sum of the singular and regular pressure distributions obtained as solutions of the downwash integral equation operating on the j^{th} deflection mode shape.

$$\Delta P_j(\xi,\eta) = \Delta P_{r_j}(\xi,\eta) + \Delta P_{s_j}(\xi,\eta) \qquad (77)$$

The regular pressure distribution is given as

$$\Delta P_{r_j}(\xi,\eta) = 4\rho V^2 \sqrt{s^2-\eta^2} \sum_n \sum_m a_{nm}^{(j)} f_r^{(n)}(\eta)\, g_r^{(m)}(\xi,\eta) \qquad (78)$$

where $a_{nm}^{(j)}$ are the pressure coefficients obtained from the integral equation solution using the modified downwash distribution as boundary conditions for the j^{th} mode.

$f_r^{(n)}(\eta)$ represents the spanwise pressure mode distribution given in equation (55).

$g_r^{(m)}(\xi,\eta)$ represents the chordwise pressure mode distribution of equation (56).

The singular pressure distribution is given as:

$$\Delta P_{s_j}(\xi,\eta) = 4\rho V^2 \sqrt{s^2-\eta^2} \sum_{k=1}^{4} A_{(k-1)}^{(j)}\, f_s(\eta)\, g_s(\xi,\eta) \qquad (79)$$

where $f_s(\eta)$ is defined by equation (38a) (and equation (47)

$g_s(\xi,\eta)$ is defined by equation (39) or equation (47) depending upon the configuration being evaluated.

$A_{(k-1)}^{(j)}$ are four coefficients of the cubic polynomial used to define the spanwise twist distribution of $\Theta(\eta)$.

The pressure distributions reported by the computer program (reference 4) are referenced to the dynamic pressure and defined as:

$$\frac{\Delta P_j(\xi,n)}{\rho V^2/2} = \left[\text{ Machine Output }\right] \qquad \begin{array}{l}\text{dimensions same as used in} \\ \text{the ratio } H_j(\xi,n)/b_o\end{array} \tag{80}$$

where

$$\text{Machine Output} = 8\sqrt{s^2-n^2}\left\{\sum_n \sum_m a_{nm}^{(j)}\, f_r^{(n)}(n)\, g_r^{(m)}(\xi,n) + \sum_k A_{(k-1)}^{(j)}\, f_s(n)\, g_s(\xi,n)\right\}$$

Sectional generalized forces may be obtained at arbitrary locations along the semispan and are defined as:

$$Q_{ij}^s = \int_{b_o x_\ell}^{b_o x_t} \Delta P_j(\xi,n)\, H_i(\xi,n)\, d(b_o\xi)$$

$$= b_o \int_{x_\ell}^{x_t} \Delta P_j(\xi,n)\, H_i(\xi,n)\, d\xi \tag{81}$$

A maximum of eleven (11) sectional generalized forces may be calculated for each mode shape and are referenced to $S\rho V^2/2$.

$$\frac{Q_{ij}^s}{S\rho V^2/2} = \left[\text{ Machine Output }\right] \qquad \begin{array}{l}\text{dimensions same as used} \\ \text{in } H_j(\xi,n)\end{array} \tag{82}$$

(note: $b_o s = S$ length of semispan)

where

$$\left[\text{Machine Output}\right] = 8 \int_{x_\ell}^{x_t} H_i(\xi,\eta) \sqrt{1-(\tfrac{\eta}{s})^2} \left\{ \sum_n \sum_m a_{nm}^{(j)} f_r^{(n)}(\eta)\, g_r^{(m)}(\xi,\eta) + \sum_k A_{(k-1)}^{(j)} \frac{f_s(\eta)}{s} g_s(\xi,\eta) \right\} d\xi$$

The total generalized forces are evaluated using the definition:

$$Q_{ij} = b_o^2 \int_0^s \int_{x_\ell}^{x_t} \Delta P_j(\xi,\eta)\, H_i(\xi,\eta)\, d\xi d\eta \qquad (83)$$

The program output (reference 4) of generalized forces are referenced to $b_o S\rho V^2/2$ and given in the form:

$$\frac{Q_{ij}}{b_o S\rho V^2/2} = \left[\text{Machine Output}\right] \quad \begin{matrix} \text{same dimensions as used in} \\ H_j(\xi,\eta) \end{matrix} \qquad (84)$$

(note: $b_o^2 s = b_o S$)

where

$$\left[\text{Machine Output}\right] = 8 \int_0^s \int_{x_\ell}^{x_t} H_i(\xi,\eta) \sqrt{1-(\tfrac{\eta}{s})^2} \left\{ \sum_n \sum_m a_{nm}^{(j)} f_r^{(n)}(\eta)\, g_r^{(m)}(\xi,\eta) + \sum_k A_{(k-1)}^{(j)} \frac{f_s(\eta)}{s} g_s(\xi,\eta) \right\} d\xi d\eta$$

It should be noted that the sectional generalized forces (equation (82)) are used to obtain information on the spanwise loadings and chordwise center of pressure locations. The maximum number of stations where the sectional forces are calculated is limited to eleven (11), and the spanwise distribution is selected by the user.

The spanwise locations (where the sectional generalized forces are calculated) do not coincide with spanwise quadrature stations where the chordwise integrals of equation (84) are evaluated. The chordwise integrals

of equation (84) are calculated at particular spanwise stations depending upon the quadrature distribution required for a particular configuration and are not printed as output.

PROGRAM CAPABILITIES AND LIMITATIONS

The computer program developed around the preferred solution process may be used for a vast array of analysis configurations and has capabilities and limitations listed below:

1. Trailing edge control surface configurations may be composed of a full span, inboard partial-span, outboard tip partial-span, or up to four individual control surfaces including side-by-side common edge control surfaces.
2. All hingelines are assumed to be located at the leading edge of the control surfaces. Control surface hingelines may have individual definitions, however, each hingeline is assumed to be defined by a linear equation.
3. All control surface leading edges and inboard side edges are assumed to be represented by a sealed gap condition.
4. All control surface side edges are assumed to be parallel to the remote stream direction.
5. Spanwise elastic twist distribution of the control surface hingeline is approximated by a cubic polynomial to allow a spanwise variation of the hingeline rotation $\Theta(\eta)$.
6. Control surface camber bending is treated within the regular lifting surface solution.
7. Lifting surface solutions of planforms not having control surfaces may be obtained upon user option.
8. Spanwise symmetrical or antisymmetrical analysis may be accomplished upon user option.

9. Planform definition is assumed to consist of linear segments defined by input data. (See Appendix A on effect of locating downwash chords near junctions of linear segments of planform definition.)

10. Downwash boundary conditions may be modified to include local streamwise velocity variations due to airfoil thickness effects. (See Appendix A) (See reference 4 for limitations)

11. Input mode shapes may be defined at many points on the surface (such as obtained from a finite element structural analysis)--or optionally may be defined using distortion shapes of an elastic axis modal analysis (see Appendix A of reference 4).

12. Multiple k value and Mach number analyses may be made in a single machine run (See reference 4, Section 3.7.2 LIMITATIONS)

13. The printed output of the program, obtained on user option, consists of a definition of kinematic downwash matrix, mathematical discontinuous downwash matrix, modified downwash matrix, pressure series coefficients, chordwise array of pressures at prescribed spanwise stations, sectional generalized forces, and total generalized forces.

RESULTS, COMPARISONS AND DISCUSSION

This section contains an illustration of the downwash subtraction procedure used in the preferred solution process and also provides pressure distributions and generalized forces resulting from analysis of four wing-control surface configurations for which experimental data are available for comparison. The four experimental configurations consist of (1) the swept-wing full span flap configuration of reference 12 that provides pressures due to a steady flap deflection, (2) a swept-wing having an inboard partial span control surface of reference 13 for which non-oscillatory pressures are available, (3) a non-swept rectangular wing having an oscillating full span flap (reference 14), and (4) a swept wing having side-by-side control surfaces oscillating in various arrangements (reference 15).

Description of Downwash Subtraction Process

The configuration of reference 15, shown in figure 16, is used to illustrate the downwash subtraction process.

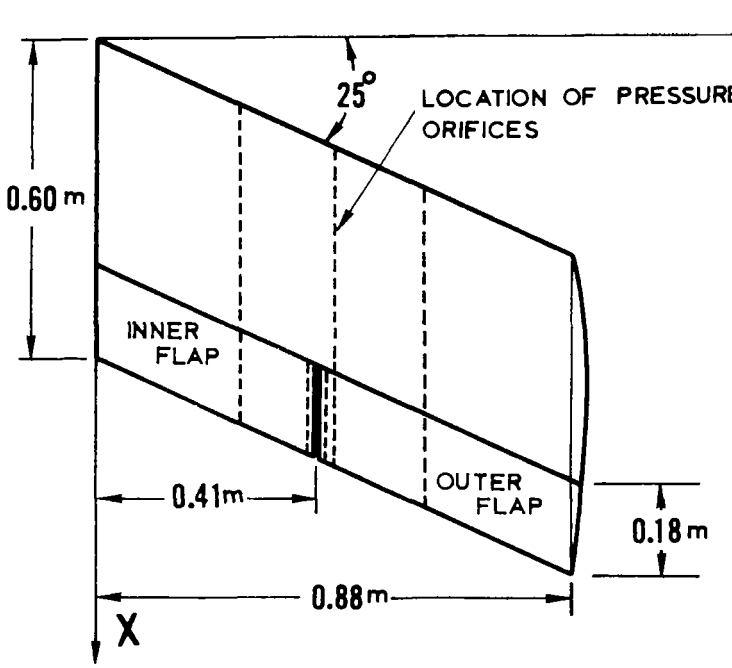

Figure 16.- Experimental Planform of Reference 15 Showing the Side-by-Side Control Surface Arrangement (dimensions in meters)

The inboard control surface is assumed to be oscillating about its hingeline at a reduced frequency of k = 0.372 and at a Mach number of M = 0. The rotation angle is assumed to be constant across the span of the control surface having a value of one radian measured in a plane perpendicular to the y axis. Remaining portion of the lifting surface is assumed to be at rest. It is also assumed that the control surface motions are spanwise symmetrical with respect to the planform center line. The subtraction process is illustrated only for the in-phase part of the downwash distribution.

The in-phase part of the kinematic downwash distribution obtained from the motion definition is shown in figure 17 for nine chords equally spaced across the semispan. The downwash has a uniform value of $\frac{\bar{w}}{V}$ = 1.0 over the control surface and is zero everywhere else.

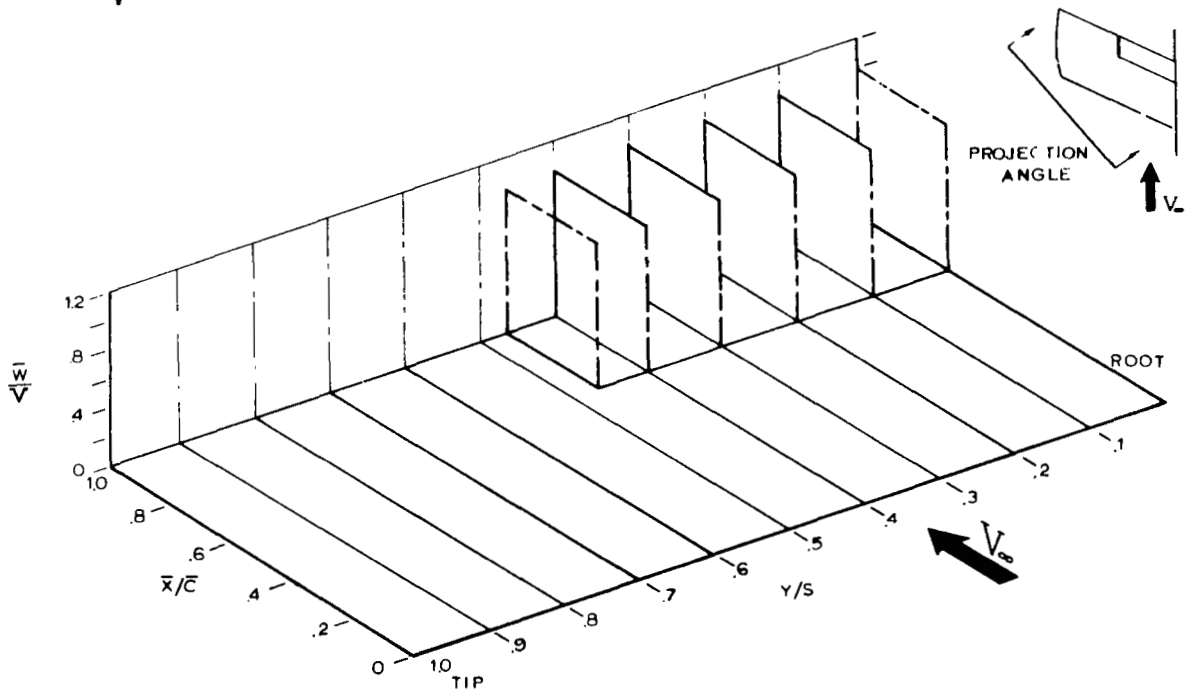

Figure 17.- Kinematic Downwash Distribution Derived from Motions of Inboard Flap

Downwash distribution resulting from the integral evaluation using the loading functions defined by equation (38) is shown in figure 18. The distributions are smooth in regions outside of the control surface and a unit change in downwash across the hingeline is obtained for the chords that lie on the control surface.

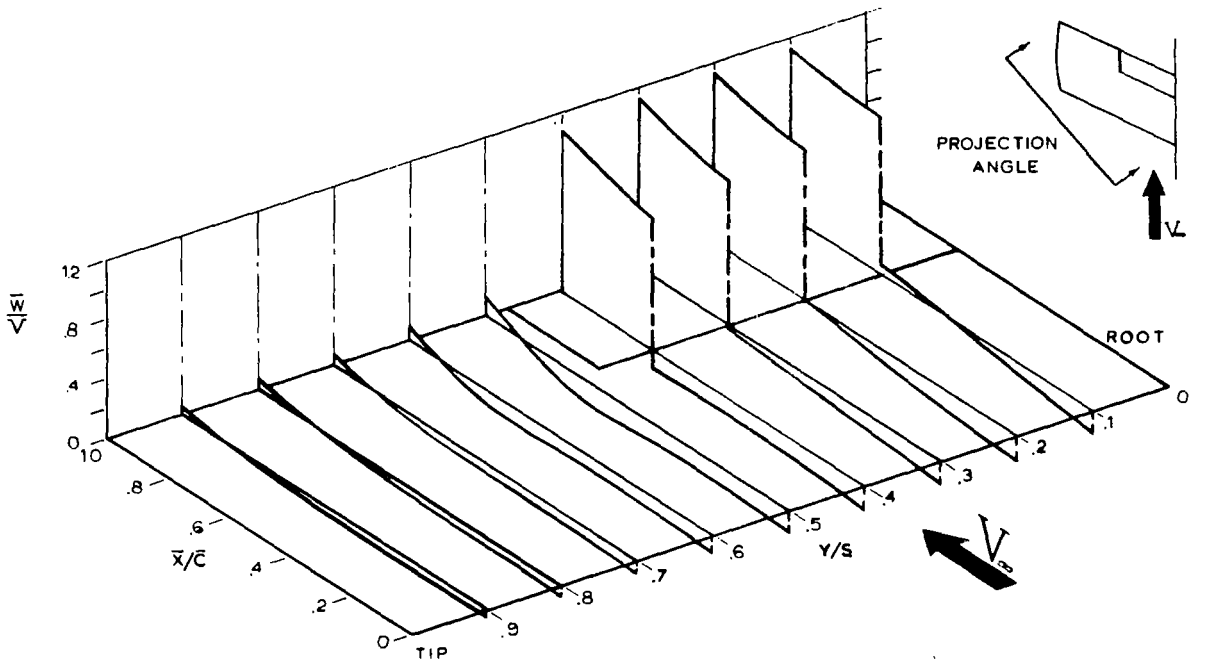

Figure 18.- Derived Downwash Distribution Obtained from the Integral Evaluation Using Loading Functions of Equation (38)

The downwash distribution of figure 18 is subtracted from the kinematic distribution of figure 17 resulting in the modified distribution of figure 19.

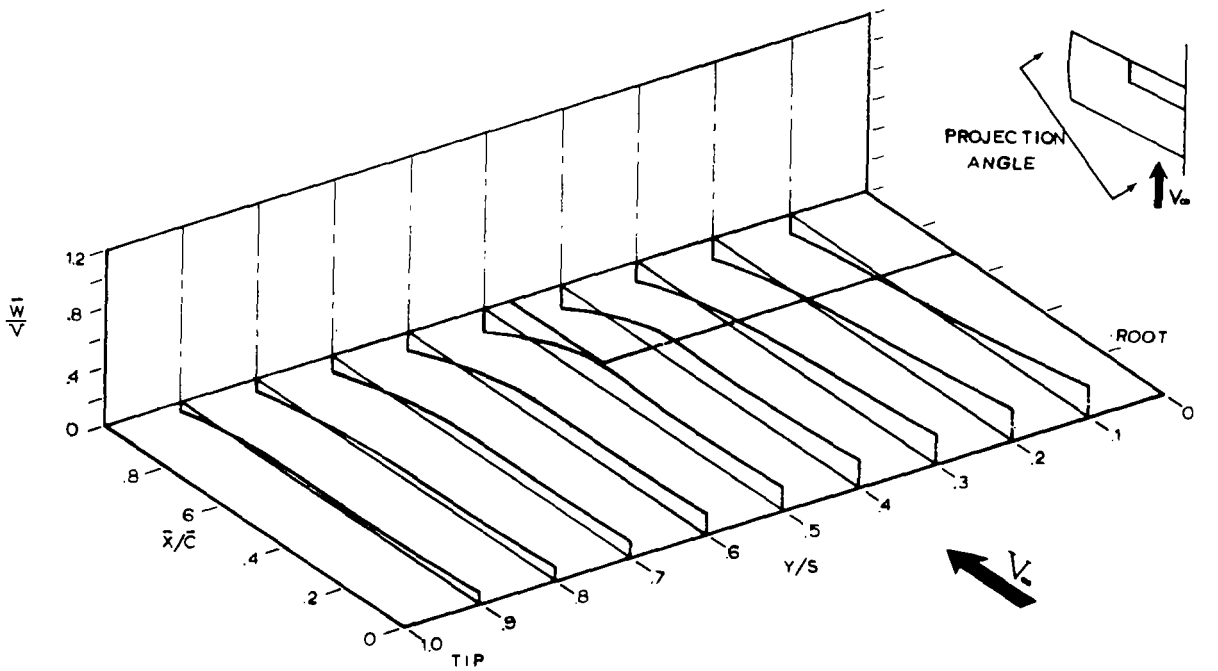

Figure 19.- Modified Downwash Distribution Obtained by Subtracting the Derived Distribution from Kinematic Distribution

Since the modified distribution is smooth and does not contain any discontinuities, it appears that the pressure loading functions (equation (38)) that were developed from the asymptotic expansion process of reference 3 provide the proper description of surface loadings to be used in obtaining solutions for configurations having discontinuous downwash distributions.

Steady-State Results for Full-Span Flap Configuration

The full-span flap configuration of reference 12 is shown in figure 20 for which experimental pressures were obtained for various combinations of flap deflections and wing angles of attack. The flap deflection and wing angle of attack were maintained at constant values for each experimental run.

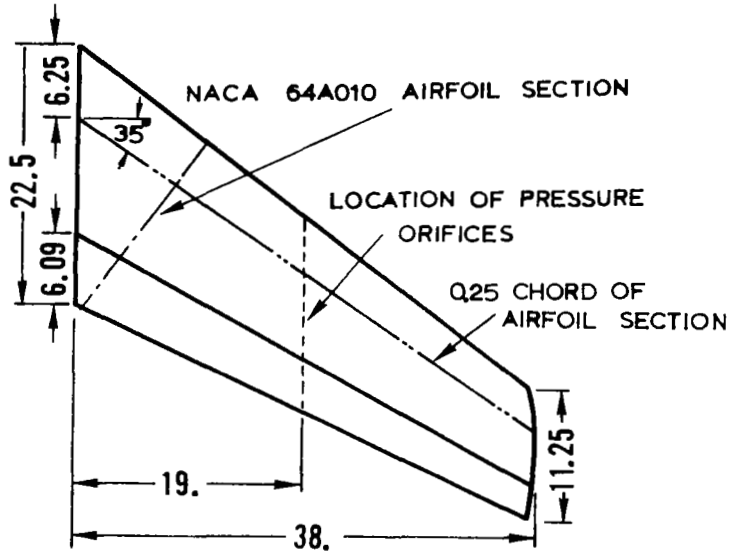

Figure 20.- Experimental Full-Span Flap Configuration NACA RM A9G13 (dimensions in inches)

Experimental pressures were obtained along a streamwise section located at the 50% semispan station. The longitudinal junction between the wing and flap was sealed to prevent flow leakage between the lower and upper surfaces at the hingeline.

The theoretical pressure distributions are obtained using a modification on the boundary conditions (described in Appendix A) that include local streamwise velocity variations due to airfoil thickness effects. A comparison of the experimental and theoretical results are shown in figure 21.

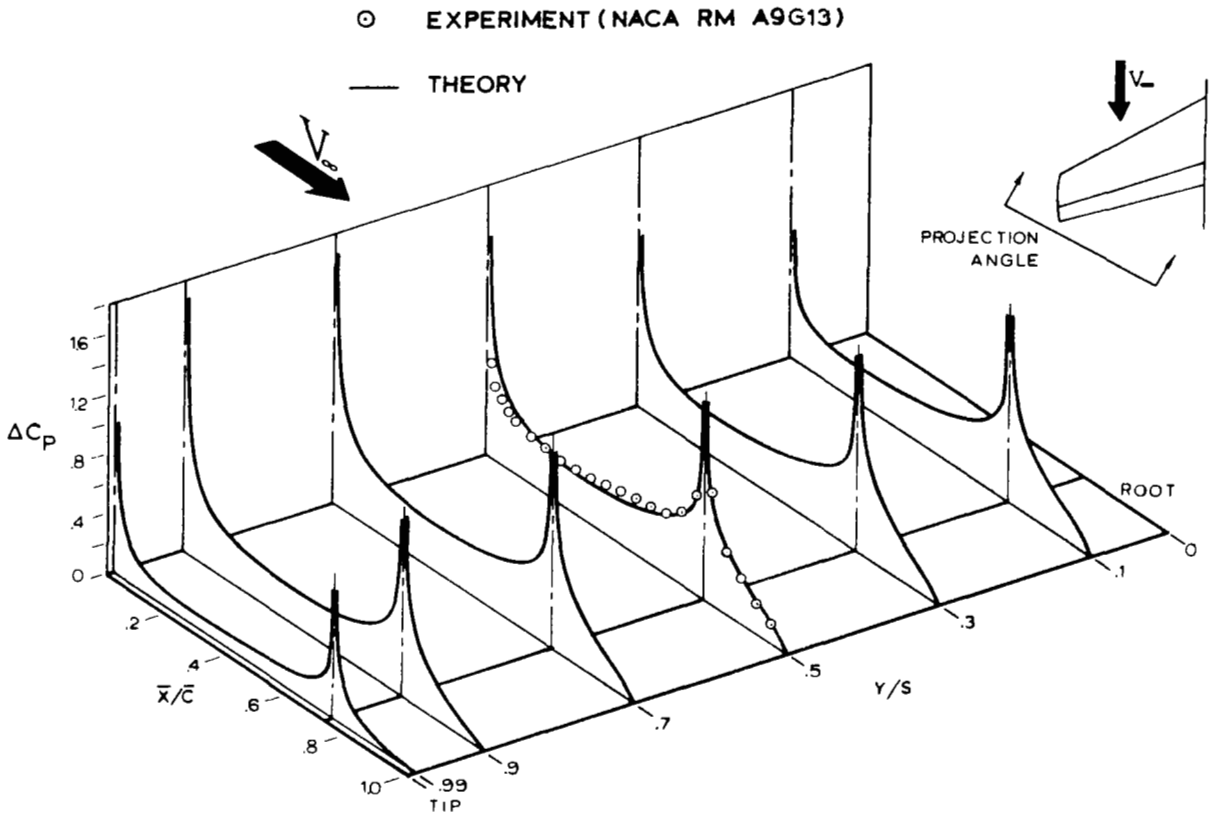

Figure 21.- Theoretical and Experimental Chordwise Pressure Distributions for a Full-Span Flap Deflected by δ = 10°, α = 0.0° at M = 0.21 and k = 0

The experimental sealed gap condition at the hingeline satisfies the theoretical assumptions (reference 3) and provides a one-to-one basis for evaluating the accuracy of the theoretical prediction method.

The comparison indicates that the experimental values are theoretically predicted within very close tolerances over the entire length of the chord even in the vicinity of the hingeline.

Steady-State Results for a Partial-Span Flap Configuration

The partial-span control surface configuration shown in figure 22 represents the experimental planform of reference 13 to obtain chordwise pressure distributions due to a steady flap deflection. Pressures were obtained along a streamwise chord located at the 46% semispan station. The hingeline gap was sealed providing a one-to-one basis for comparing theoretical and experimental results.

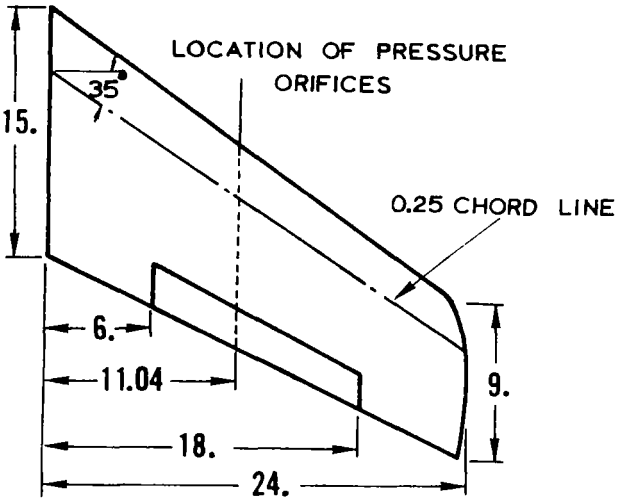

Figure 22.- Experimental Planform of a Partial-Span Flap Configuration of NACA RM L53C23 (dimensions in inches)

Theoretical pressures were obtained along various streamwise chords spaced over the semispan and are shown in figure 23. The comparison indicates that the experimental pressures are accurately predicted by the theoretical technique over the length of the chordwise strip forward of the hingeline. The theoretical distribution over the control surface are only slightly larger than the experimental values. Consequently, it appears that the lifts and hinge moments may be predicted within reasonable accuracy limits for configurations having a sealed gap at the wing-control surface junction.

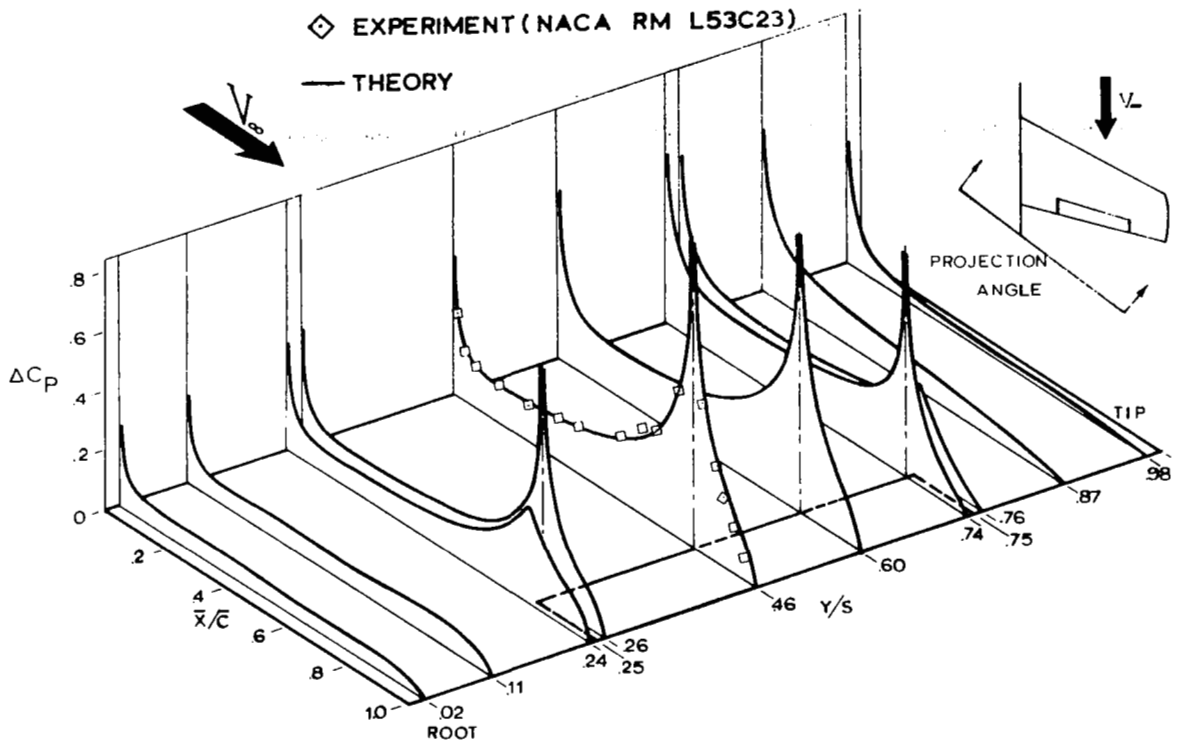

Figure 23.- Theoretical and Experimental Chordwise Pressure Distributions for Partial-Span Flap Deflected by $\delta = 10°$, $\alpha = 0°$, at M = 0.60 and k = 0

Rectangular Planforms having Full-Span Control Surfaces

Two rectangular planforms having aspect ratios of 1.0 and 2.0 were tested in combination with a 40% chord flap for various values of reduced frequencies to obtain hinge moments and lifts due to the control surface motions. The experimental data are reported in reference 14. Each planform had a small gap along its hingeline that may have a small influence on the pressure distributions in regions near the hingeline. There are no means available to determine to what extent that the pressures are affected by open gap condition since only experimental hinge moments and total lifts are available for comparison.

Experimental and theoretical values of hinge moments and phase angles as a function of reduced frequency are presented in figure 24 for the aspect ratio 2.0 planform. The theoretical hinge moments appear to agree with the experimental values, however there is a discrepancy in the predicted phase angles that may be due to the open gap at the hingeline.

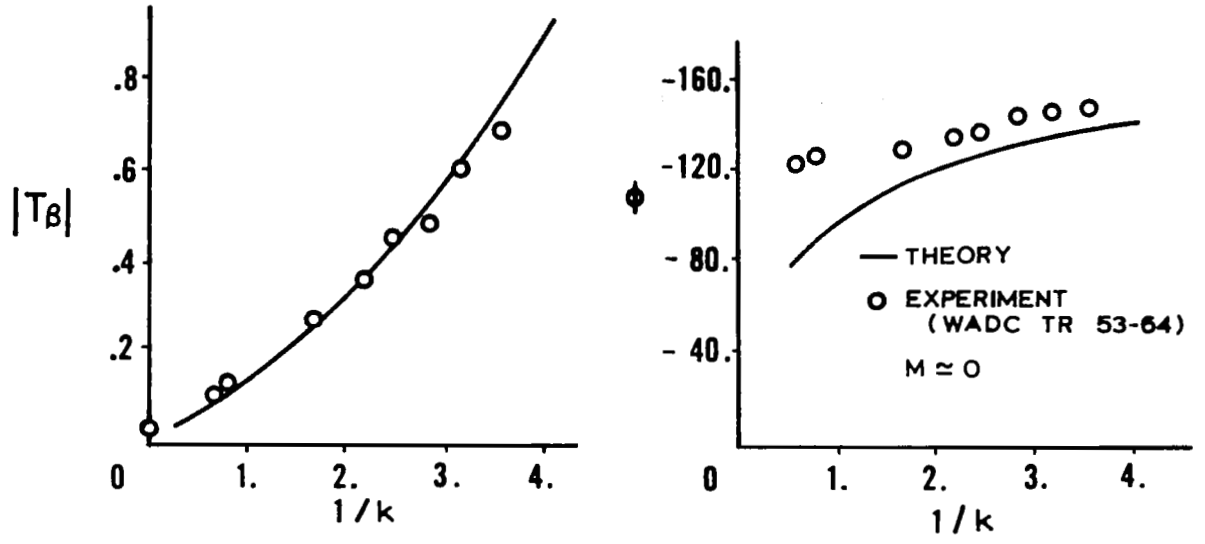

Figure 24.- Theoretical and Experimental Hinge Moments and Phase Angles for an Oscillating Full-Span Flap AR = 2.0 Configuration of WADC TR 53-64

Comparison of wing lifts and phase angles are shown in figure 25. There is good agreement between the theoretical and experimental results over the entire range of reduced frequencies used in the tests. Consequently, it appears that wing lift is not greatly affected by open gaps at the hingeline.

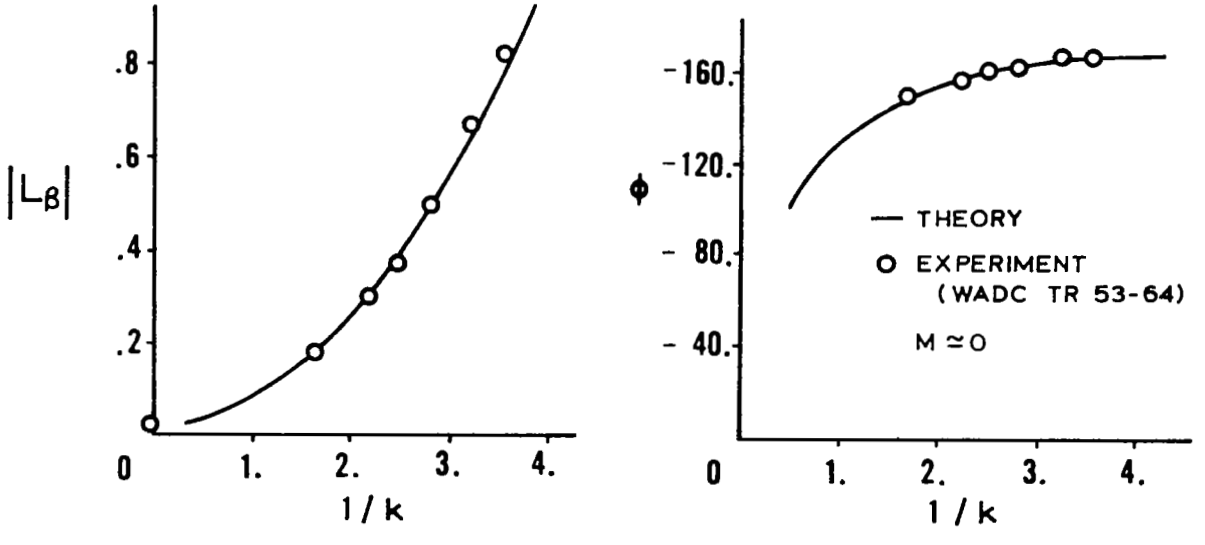

Figure 25.- Theoretical and Experimental Lifts and Phase Angles for an Oscillating Full-Span Flap AR = 2.0 Configuration of WADC TR 53-64

Experimental and theoretical results for the full span control surface configuration of aspect ratio 1.0 are shown in figure 26 and figure 27. Again, the theoretical method appears to predict reasonable values of hinge moments and total lifts; however, the predicted hinge moment phase angles deviate from the experimental values and the discrepancy may be due to the open gap at the hingeline.

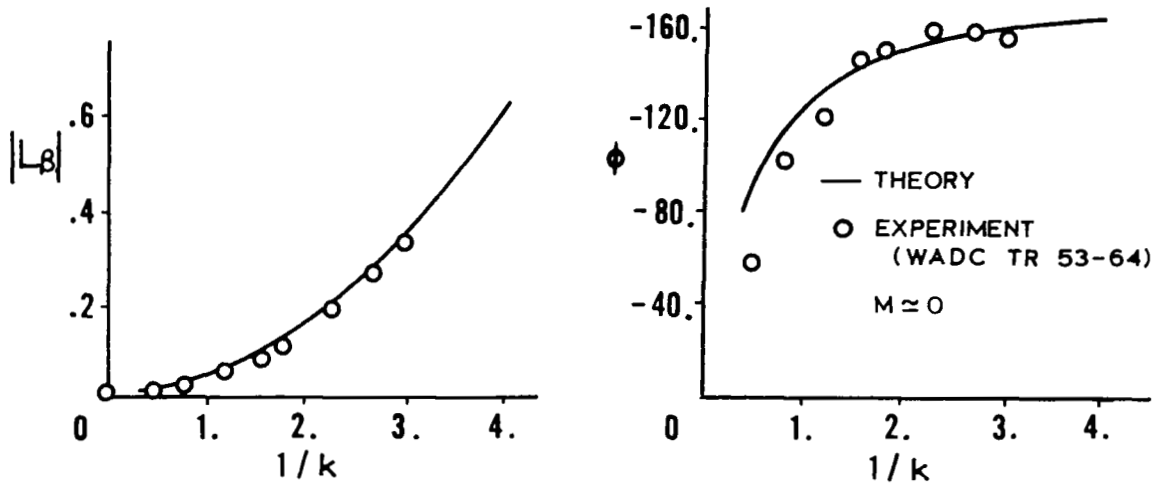

Figure 26.- Theoretical and Experimental Lifts and Phase Angles for an Oscillating Full-Span Flap AR = 1.0 Configuration of WADC TR 53-64

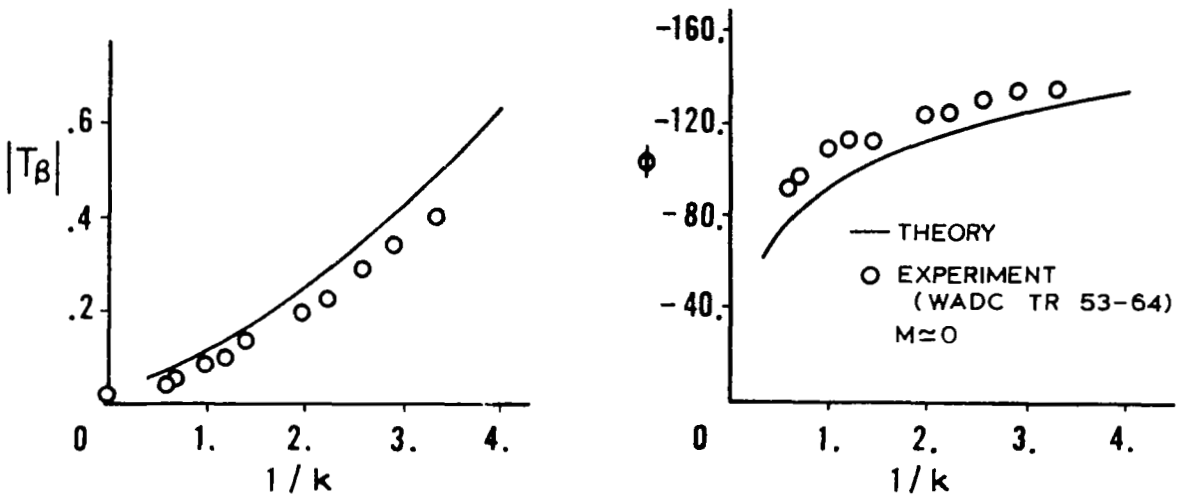

Figure 27.- Theoretical and Experimental Hinge Moments and Phase Angles for an Oscillating Full-Span Flap AR = 1.0 Configuration of WADC TR 53-64

The difference may also be caused by trailing edge flow separation that could have been experienced during the test since there is a very large adverse pressure gradient at the trailing edge that might not have been maintained during the experiment. (see page 315 of reference 17 for the pressure gradient plot of the NACA 0010 airfoil section used in the experiment.)

Effect of Hingeline Gaps on Chordwise Loadings

A theoretical study has been made (reference 16) to investigate the effect of hingeline gaps on chordwise pressure distribution, and the results are shown in figure 28.

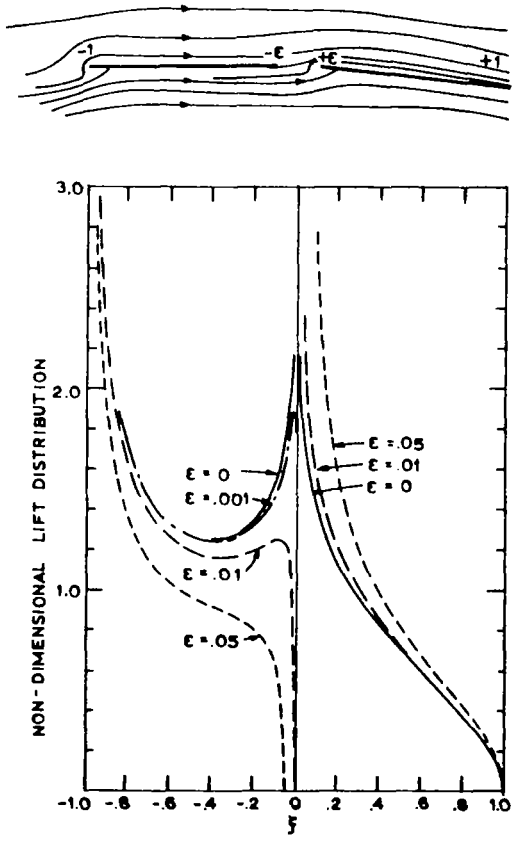

Figure 28.- Non-Dimensional Lift Distribution (reproduced from reference 16)

The study configuration is composed of a pair of two-dimensional equal chord lifting surfaces that are placed in a coplanar arrangement. The leading surface is at a zero angle of attack and the trailing surface is given an angle of attack by rotating the surface about its leading edge. Chordwise pressures are obtained for various separation spacings in steady flow.

For a zero gap spacing the loadings produced at the junction of the two surfaces exhibit the typical symmetrical logarithmic singularity identified for a discontinuous downwash distribution of a two-dimensional wing-control surface combination. As separation begins, the loadings on the wing near the wing trailing edge change from a singularity characteristic to a loading that becomes equal to zero. However, the loadings near the leading edge of the control surface change from a logarithmic characteristic to that of having an inverse square root singularity that causes a higher loading to exist on the control surface for the open gap condition than for the zero gap condition.

Large separation distances between the surfaces result in loadings that are vastly different from the zero separation case. However, small separations affect the pressure distributions only in localized regions near the hingeline. It appears that the zero gap theoretical method will provide reasonable predictions of total lifts and moments for configurations having small hingeline gaps.

Side-by-Side Control Surface Configuration

The side-by-side control surface configuration is shown in figure 16 for which unsteady pressures are obtained for various combination of flap deflections. The experimental model had small open gaps at the hingelines and at the side edges. Reference 15 provides no information to define the exact dimensions between the control surface side edges and the pressure measuring stations located in the vicinity of the side edges. The spanwise location of the experimental pressure chords were established by measuring the pressure chord locations off of the planform drawing.

Figures 29 and 30 present comparisons of theoretical and experimental results for a mode shape in which both flaps are oscillating with the same phase and amplitude and the wing is maintained in a stationary position. There is good agreement between the theoretical and experimental results in all areas except in localized regions near the hingelines. The experimental values are less than the theoretical values forward of the hingeline and slightly greater than the predicted valuse aft of the hingeline. The variations near the hingeline are attributed to the open gaps at the hingelines. Even though the comparisons deteriorate in regions near the hingeline it appears that the total lifts and moments may be estimated within reasonable bounds for configurations that have small open gaps at the hingelines.

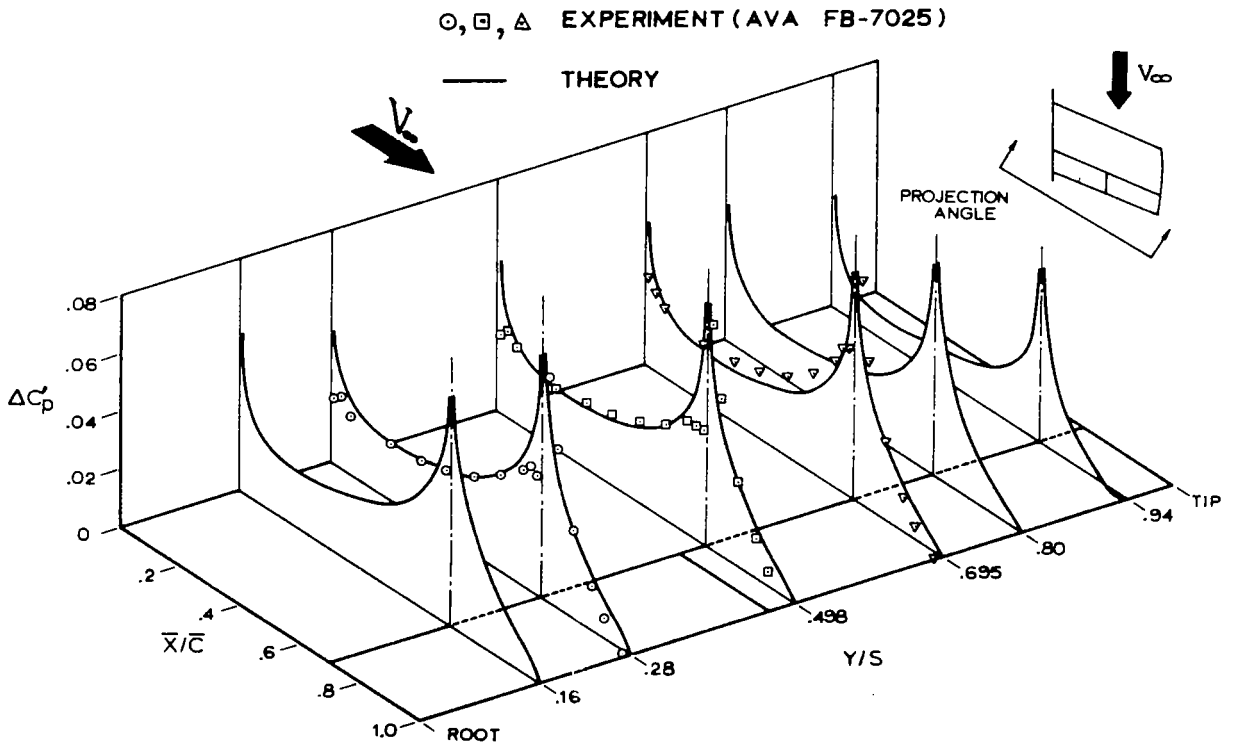

Figure 29.- In-Phase Chordwise Pressure Distributions for Both Flaps Oscillating with the Same Phase and Amplitude. $A_{i.f.} = 0.82°$, $A_{o.f.} = 0.82°$, $A_w = 0°$, $k = 0.372$, and $M \simeq 0$

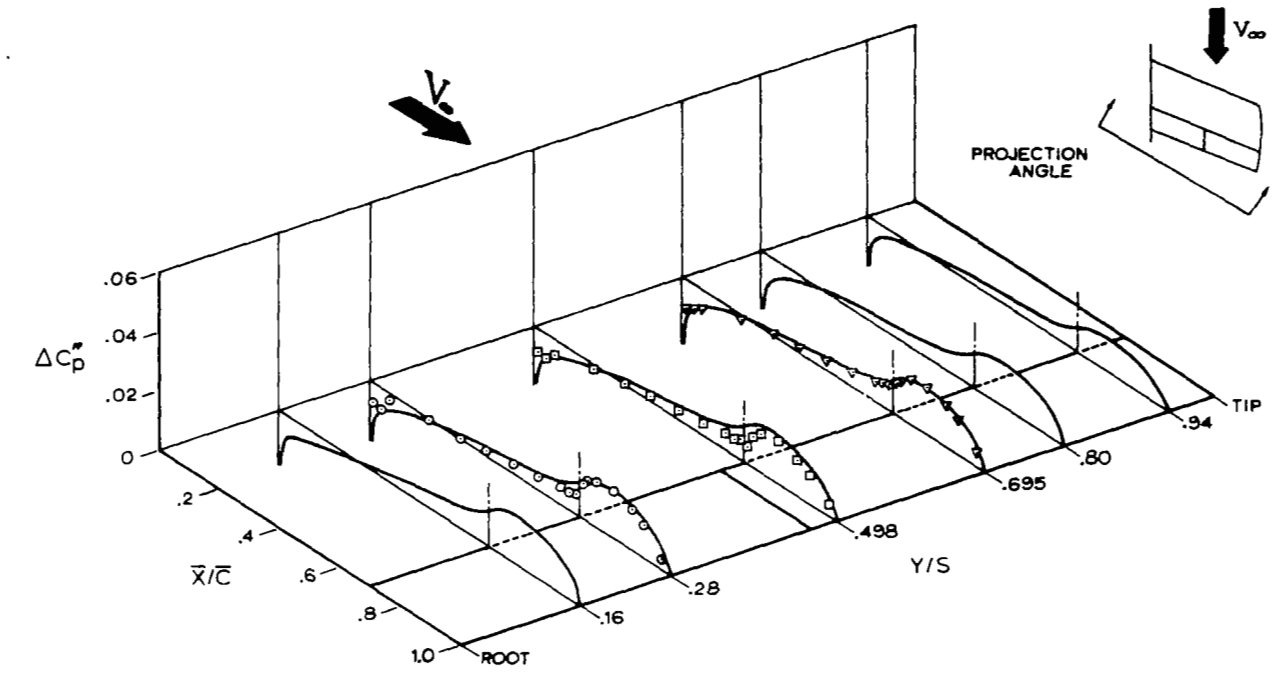

Figure 30.- Out-of-Phase Chordwise Pressure Distributions for Both Flaps Oscillating with the same Phase and Amplitude. $A_{i.f.} = 0.82°$, $A_{o.f.} = 0.82°$, $A_w = 0°$

Figures 31 and 32 present comparisons of theoretical and experimental pressure distributions for a mode shape in which the outer flap is oscillating and the inner flap and wing are maintained in a stationary position.

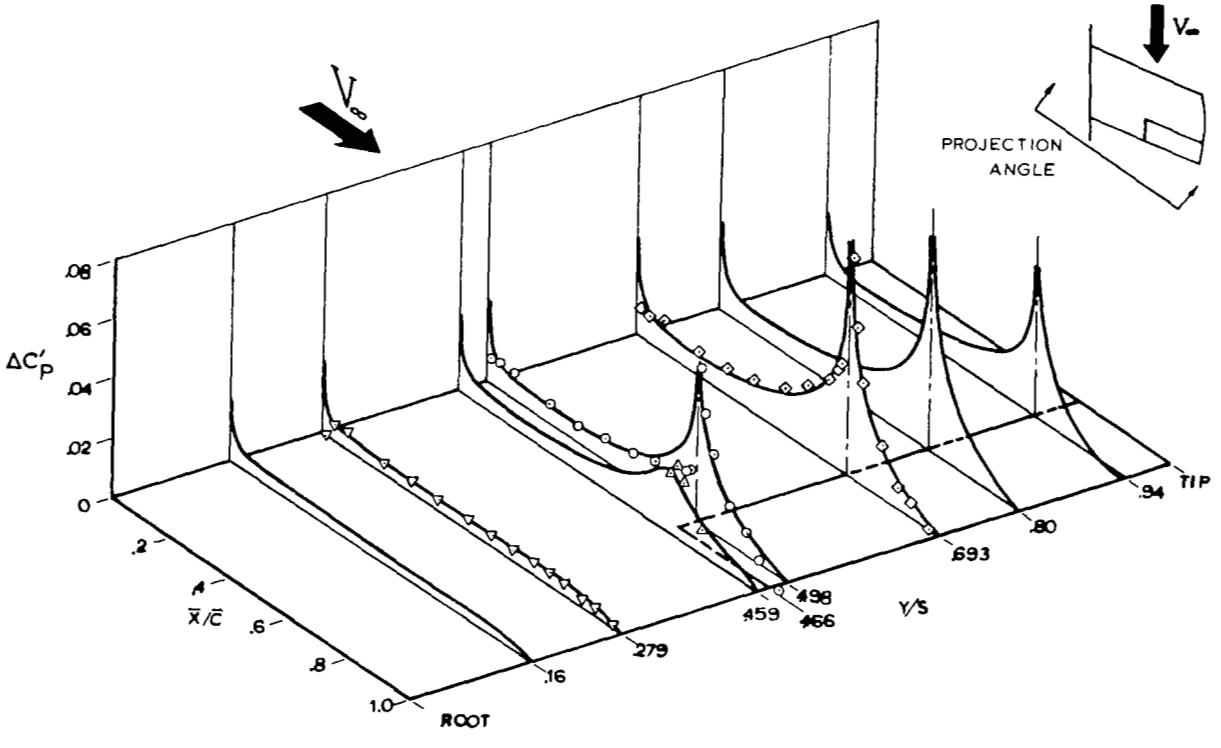

Figure 31.- In-Phase Chordwise Pressure Distributions Resulting from Motions of Outer Flap. $A_{i.f.} = 0°$, $A_{o.f.} = 0.66°$, $A_w = 0°$, $k = 0.372$, and $M \simeq 0$

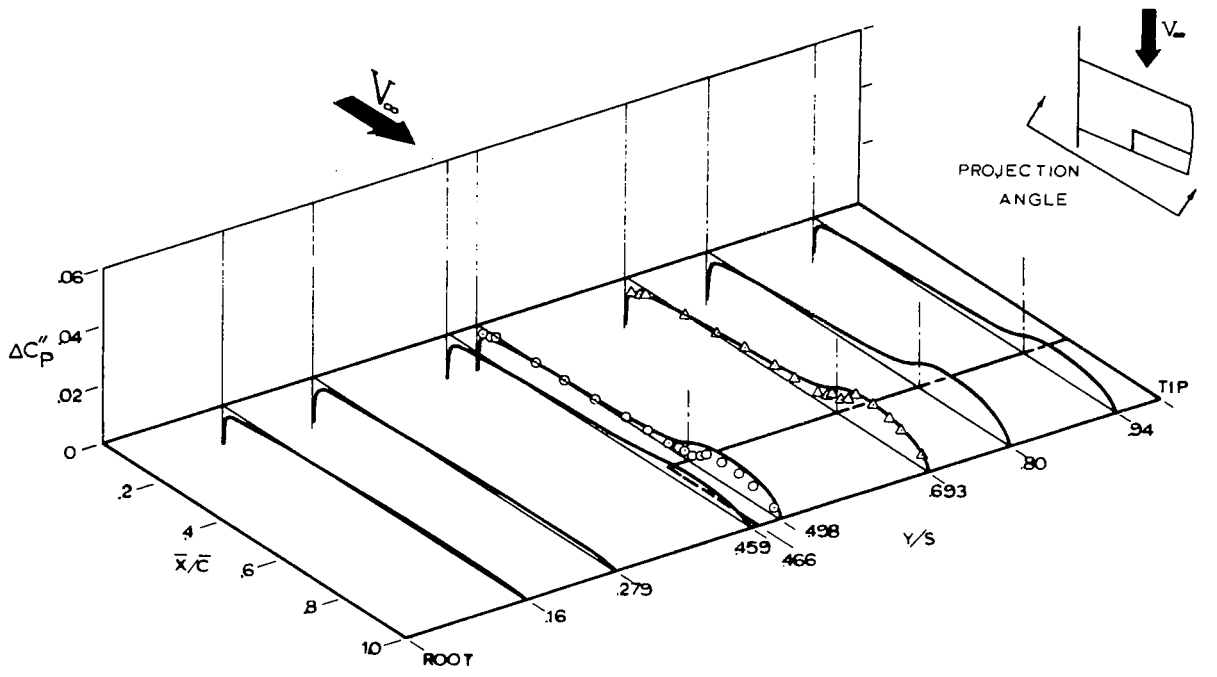

Figure 32.- Out-of-Phase Chordwise Pressure Distributions Resulting from Motions of Outer Flap. $A_{i.f.} = 0°$, $A_{o.f.} = 0.66°$, $A_w = 0°$, $k = 0.372$, and $M \simeq 0$

Again, the only area where the comparisons deteriorate is within the hingeline region and is probably due to open gap effects at the hingeline.

CONCLUSION

A theoretical analysis and computer program have been developed for the prediction of unsteady lifting surface loadings caused by motions of trailing edge control surfaces having sealed gaps. The program has been developed around a systematic solution process where the discontinuities in the downwash distributions are separated (and handled separately) prior to applying standard lifting-surface solution techniques.

Theoretical results are presented to demonstrate the versatility of the program capabilities. Comparisons of theoretical and experimental data are presented for four wing-control surface configurations. Two of the experimental configurations had sealed gaps at the hingelines, and two configurations had small open gaps.

The comparisons indicate that reasonable pressure distributions are obtained for the sealed gap cases, but there are moderate differences near the hingelines for the open gap cases.

The results also indicate that the method developed will provide reasonable predictions of unsteady loadings for a great variety of control surface configurations.

REFERENCES

1. A. H. FLAX: Reverse Flow and Variational Theorems of Lifting Surface in Nonstationary Compressible Flow. J. Aeron. Sci. (1953), pp. 120-126.

2. J. H. BERMAN, P. SKYPPYKEVICH, J. B. SMEDFIELD: Unsteady Aerodynamic Forces in General Wing/Control. Surface Configuration in Subsonic Flow. AFFDL-TR-67-117.

3. M. LANDAHL: "Pressure Loading Functions for Oscillating Wings with Control Surfaces" AIAA Journal, Vol. 6, No. 2, Feb. 1968.

4. M. C. REDMAN, W. S. ROWE, B. A. WINTHER: Prediction of Unsteady Aerodynamic Loadings caused by Trailing Edge Control Surface Motions in Subsonic Compressible Flow--Computer Program Description, NASA CR-112015.

5. H. G. KUSSNER: General Lifting Surface Theory, Luftfahrtforschung, Vol. 17, No. 11/12, Dec. 10, 1940. Also discussed in Aerodynamic Flutter, I. E. Garrick, editor. AIAA Selected Reprints, Vol. V

6. C. E. WATKINS, H. L. RUNYAN, D. S. WOOLSTON: On the Kernel Function of the Integral Equation Relating the Lift and Downwash Distributions of Oscillating Finite Wings in Subsonic Flow. NACA Rep. 1234.

7. P. T. HSU: "Calculation of Pressure Distributions for Oscillating Wings of Arbitrary Planform in Subsonic Flow by the Kernel Function Method" MIT ASRL T.R. 64-1.

8. H. MULTHOPP, "Methods for Calculating the Lift Distribution of Wings (Subsonic Lifting-Surface Theory)" ARC R & M 2884.

9. B. LASCHKA, Zur Theorie der harmonish schwingenden tragenden Flache bez Unterschallstromung. Z. Flugwiss 12 (1963), pages 265-292.

10. H. ASHLEY and W. S. ROWE: "Unsteady Aerodynamic Loading of Wings With Control Surfaces". Z. Flugwiss 18 (1970). September/Oktober, pages 321-330.

11. H. FREESE: "Zur Berechnung der Ruderluftkrafte im Unterschallbereich" ZAMM 50, 633-636 (1970).

12. B. E. TINLING and J. K. DICKSON: "Tests of a Model Horizontal Tail of Aspect Ratio 4.5 in the AMES 12-foot Pressure Wind Tunnel" NACA RM A9G13.

13. A. D. HAMMOND and B. A. KEFFER: "The Effect at High Subsonic Speeds of a Flap-Type Aileron on the Chordwise Pressure Distribution Near Mid-semispan of a 35° Sweptback Wing of Aspect Ratio 4 having NACA 65A006 Airfoil Section" NACA RM L53C23.

14. V. BEALS, and W. P. TARGOFF: "Control Surface Oscillatory Coefficients Measured on Low Aspect Ratio Wings" WADC TR No. 53-64.

15. H. FORSCHING, H. TRIEBSTEIN, J. WAGENER: "Pressure Measurements on Harmonically Oscillating Swept Wing with Two Control Surfaces in Incompressible Flow" presented at Symposium Aerodynamics of Interfering Surfaces, Tonsberg, Norway (1970) AVA FB 7025.

16. R. B. WHITE and M. T. LANDAHL: "Effect of Gaps on the Loading Distribution of Planar Lifting Surfaces" AIAA Journal, April 1968, pages 626-631.

17. I. H. ABBOTT and A. E. VonDOENHOFF: "Theory of Wing Sections", McGraw-Hill Book Company (1949).

APPENDIX A

A CAUTION REGARDING PLANFORMS WITH DISCONTINUOUS EDGES, AND A PROVISION FOR INCLUDING EFFECTS OF AIRFOIL THICKNESS VIA LOCAL LINEARIZATION

Suggestions are made for modifying analytical procedures used in obtaining loadings on discontinuous planform shapes, and for modifying lifting surface boundary conditions $\bar{w}/V$ such that the physical flow pressure distributions are more readily simulated by the theoretical pressure distributions.

Modification of Planforms Having Discontinuous Shapes

Analytical difficulties may be encountered in predicting the aerodynamic loadings on planforms having analytic discontinuities in the planform shape definition. Figure 33 represents a typical analysis planform where first derivative discontinuities in the shape definition exist and may provide inconsistent results if the spanwise distribution of collocation stations contain a control point located at or very near the spanwise discontinuity station.

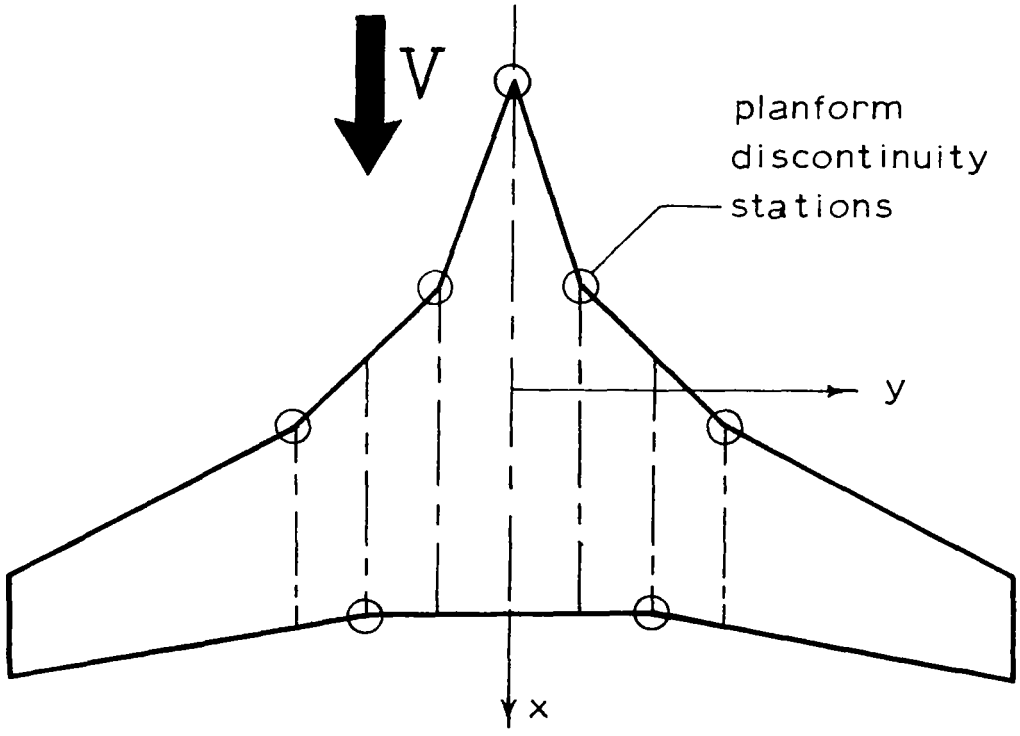

Figure 33.- Typical Analysis Configuration with a Discontinuous Shape Definition

The mathematically derived downwash sheets obtained from an evaluation of the downwash integral will exhibit singularities whenever collocation stations are located at the planform spanwise discontinuity stations. The singularities are due to the over-simplified manner in which the pressure distributions are assumed to exist over the planform. The assumed pressure functions are distributed continuously over the surface in such a manner that the planform is completely covered regardless of the analytic continuity of the planform definition. If the planform definition contains sharp breaks or discontinuities in its first derivative definition, then the pressure distributions and resulting spanwise loadings will also exhibit discontinuities at the same spanwise stations. It is the discontinuous first derivative of spanwise loadings that cause the numerical problems and produce singularities in the predicted downwash sheets. The spanwise loading discontinuities may be removed by using a suitable pressure distribution that is analytically continuous in its spanwise direction. However, no such distributions have been formulated nor used within the present program development since it is obvious that there are other means available for obtaining reasonable results other than overemphasizing the effects of localized flow in regions of planform discontinuities. The problem of downwash singularities may be circumvented by smoothing the planform discontinuities or by keeping the spanwise location of collocation stations well away from the troublesome regions. However, numerical problems do exist and the analyst should be cognizant of the potential problem and to what extent that the downwash distributions may be distorted in the regions of planform discontinuities.

The extent of downwash distortion may be determined by evaluating the downwash integral equation for the steady flow case given the following form:

$$W(x, y) = \int_{-s}^{s} \frac{\partial}{\partial \eta} \left\{ f(\eta) \int_{x_\ell}^{x_t} g(\xi,\eta) \left[1 + \frac{x-\xi}{\sqrt{(x-\xi)^2 + \beta^2 (y-\eta)^2}} \right] d\xi \right\} \frac{d\eta}{y-\eta} \qquad (A1)$$

In this example, $f(\eta)$ is taken to be the spanwise pressure function corresponding to an ellipse, $f(\eta) = \sqrt{s^2 - \eta^2}$; and $g(\xi,\eta)$ is the chordwise pressure function given as

$$g(\xi,\eta) = [\, x_t(\eta) - \xi \,]^{1/2} \,/\, [\, \xi - x_\ell(\eta) \,]^{1/2}$$

Also, the planform being evaluated is a delta wing having a discontinuous planform definition at the center line.

Performing the indicated differentiation with respect to η in equation (A1) and retaining only the essential terms that contribute to the singularity problem results in the following expression:

$$\overline{W}(x, y) = \int_{-s}^{s} \left\{ \int_{x_\ell}^{x_t} f(\eta) \frac{\partial g(\xi,\eta)}{\partial \eta} \left[1 + \frac{x-\xi}{\sqrt{(x-\xi)^2+\beta^2(y-\eta)^2}} \right] d\xi \right\} \frac{d\eta}{y-\eta} \qquad (A2)$$

The $\frac{\partial g(\xi,\eta)}{\partial \eta}$ term has a finite discontinuity at the planform center line having equal but opposite signs on either side of the center line.

To shorten the expression let the chordwise integral be defined as:

$$H(\eta) = \int_{x_\ell}^{x_t} f(\eta) \frac{\partial g(\xi,\eta)}{\partial \eta} \left[1 + \frac{x-\xi}{\sqrt{(x-\xi)^2+\beta^2(y-\eta)^2}} \right] d\xi \qquad (A3)$$

And let $H_\ell(\eta)$ be $H(\eta)$ when the left hand side derivative of $\frac{\partial g(\xi,\eta)}{\partial \eta}$ used in equation (A3); also let $H_r(\eta)$ be $H(\eta)$ of equation (A3) using the right hand side derivative of $\frac{\partial g(\xi,\eta)}{\partial \eta}$

Then the shortened form of equation (A2) becomes:

$$\overline{W}(x, y) = \int_{-s}^{s} H(\eta) \frac{d\eta}{y-\eta} \qquad (A4)$$

Equation (A4) may be evaluated by adding and subtracting the function $H_\ell(\eta)$ over the integration interval $0 \leq \eta \leq s$.

$$\overline{W}(x, y) = \int_{-s}^{0} H_\ell(y) \frac{d\eta}{y-\eta} + \int_{0}^{s} H_\ell(\eta) \frac{d\eta}{y-\eta} \qquad (A5)$$

$$- \int_{0}^{s} H_\ell(\eta) \frac{d\eta}{y-\eta} + \int_{0}^{s} H_r(\eta) \frac{d\eta}{y-\eta}$$

The second and third integrals of (A5) are evaluated by making a continuous extention of the definition of $\left.\frac{\partial g(\xi,\eta)}{\partial \eta}\right|_{\ell}$ across the centerline to the right hand tip at $\eta = s$.

The integrals may be combined to provide the expression

$$\bar{W}(x,y) = \int_{-s}^{s} H_{\ell}(\eta)\,\frac{d\eta}{y-\eta} - \int_{0}^{s} H_{\ell}(\eta)\,\frac{d\eta}{y-\eta} + \int_{0}^{s} H_{r}(\eta)\,\frac{d\eta}{y-\eta} \tag{A6}$$

Singularities at $\eta = y$ are removed from the integral and evaluated separately as shown by the following:

$$\begin{aligned}\bar{W}(x,y) = {} & \int_{-s}^{s} [\, H_{\ell}(\eta) - H_{\ell}(y) \,]\,\frac{d\eta}{y-\eta} + H_{\ell}(y) \int_{-s}^{s} \frac{d\eta}{y-\eta} \\ & - \int_{0}^{s} [\, H_{\ell}(\eta) - H_{\ell}(y) \,]\,\frac{d\eta}{y-\eta} - H_{\ell}(y) \int_{0}^{s} \frac{d\eta}{y-\eta} \\ & + \int_{0}^{s} [\, H_{r}(\eta) - H_{r}(y) \,]\,\frac{d\eta}{y-\eta} + H_{r}(y) \int_{0}^{s} \frac{d\eta}{y-\eta}\end{aligned} \tag{A7}$$

The only terms containing singularities (with the restriction that the downwash stations are contained in the interval $-s < y < s$) are the terms having an integral form of

$$\int_{0}^{s} \frac{d\eta}{y-\eta} \tag{A8}$$

Equation (A7) may then be expressed as having singular and non-singular terms that take the form of:

$$\bar{W}(x,y) = [\, H_{r}(y) - H_{\ell}(y) \,]\,\ln|y| + \text{Regular Terms} \tag{A9}$$

and the limiting value of $\bar{W}(x,y)$ tends to infinity as $y \rightarrow 0$.

Thus, the downwash sheet will exhibit unrealistically large values of downwashes whenever a downwash chord is placed near a planform discontinuity station and is due solely to the manner in which the pressure loadings are assumed to exist on the boundaries of the planform.

There is an obvious solution to this problem (see reference 8) in that the derivative of the spanwise loadings may be made continuous by smoothing the planform discontinuities. An example of how smoothing of planform discontinuities affects the downwash distribution is shown in figure 34.

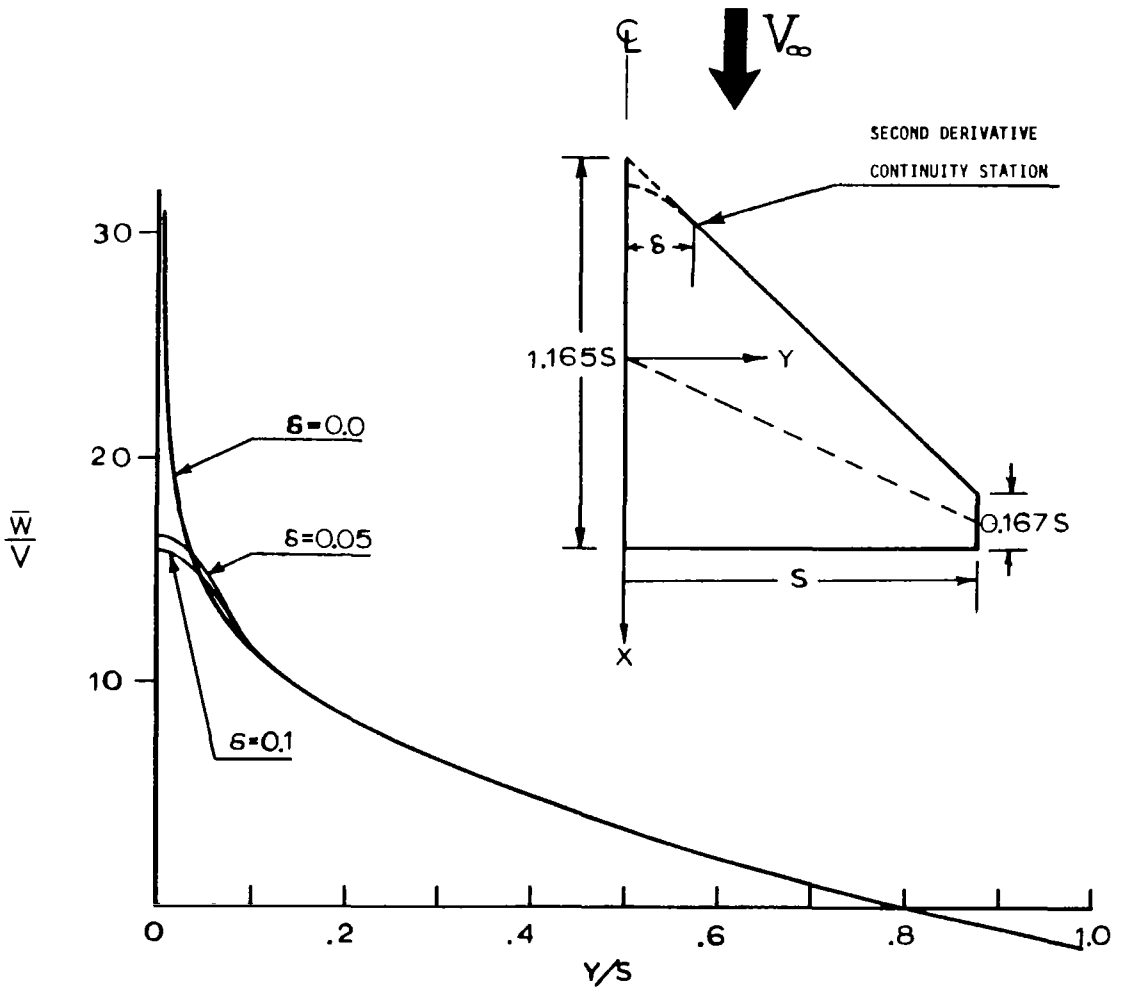

Figure 34.- Spanwise Downwash Distribution Resulting from Various Apex Smoothing Values

The clipped delta planform shown in figure 34 has been modified in the region of the apex at the centerline to produce a continuous first derivative definition of the planform across the centerline. The method selected to smooth the shape definition is one of applying a function having a continuous first derivative that is zero at the centerline and is also continuous in the second derivative at the spanwise matching station. This particular smoothing function provides derivative continuity with the least distortion in planform definition. Downwash values obtained at spanwise stations along the 50% chordline are shown in the lower part of figure 34 . The downwash distribution near the planform centerline does become singular for the pointed apex case. However, the downwashes take on more realistic values whenever the apex discontinuity is removed by applying a small amount of smoothing.

The spanwise distortion in downwash sheet is only slightly affected by redefining the planform shape. However, caution should be exercised in applying large amounts of smoothing since the redefined shape may provide a poor approximation of the original planform shape.

The above discussion has been presented to identify a potential problem that may arise in predicting the loadings on discontinuous planforms and to suggest a method to alleviate the problem. The suggested smoothing technique is not available within the present computer program, however, an alternate method is suggested such that reasonable results may be obtained without redefining the planform shape.

An alternate method suggested by other authors is one of applying engineering judgement to the placement of spanwise collocation stations in regions of planform discontinuities. The downwash distribution shown in figure 34 indicates that the distributions are only slightly affected at small distances away from the discontinuity station. The amount of distortion will be the greatest near the centerline of a highly swept planform since this is the location where the largest difference in the spanwise loading derivative exists. Planforms having leading and trailing edges defined by a combination of straight line segments for which differences in spanwise slopes are small

will produce even smaller distortions in the downwash description than is observed for the centerlines station. Consequently, it is suggested that the placement of the spanwise collocation stations (downwash chords) is such that the stations are located at least a small distance away from any planform discontinuity station.

Although application of planform smoothing or positioning of collocation stations may appear to be an artificial method to bypass the source of the problem, these methods will provide reasonable results for the aerodynamic loadings without being overly encumbered by localized flow conditions that contibute only in a small way to final load definitions.

Suggested Modification of Boundary Conditions $\bar{w}/V$

From an operational standpoint, it appears that if a local linearization is used, that is if the linearized boundary conditions $\bar{w}/V$ are modified to included local velocities due to airfoil thickness the resulting theoretical pressure distributions will simulate the physical flow conditions more accurately. Lifting surface theory solutions using assumed mode-kernel function approach usually provide results that correlate well with experimental results. An example of the correlation of theoretical-experimental results is presented for the analysis planform shown in figure 35.

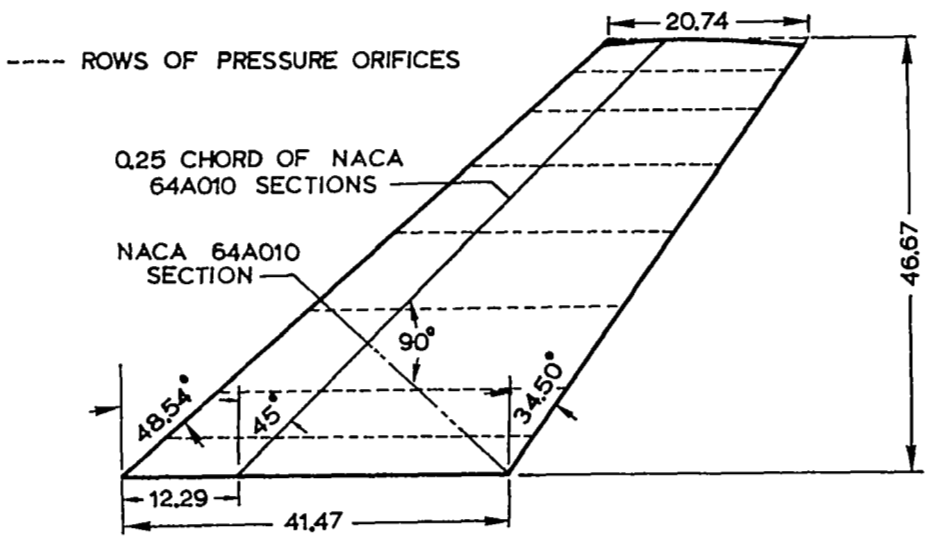

Figure 35.- Experimental Planform of NACA RM A51G31 (dimensions in inches)

Chordwise pressure distributions were obtained at seven spanwise locations as indicated in the figure. The comparisons of theoretical-experimental results are shown in figure 36 for the pressure chord located at y/s = .831 for M = 0.80 and α = 4°.

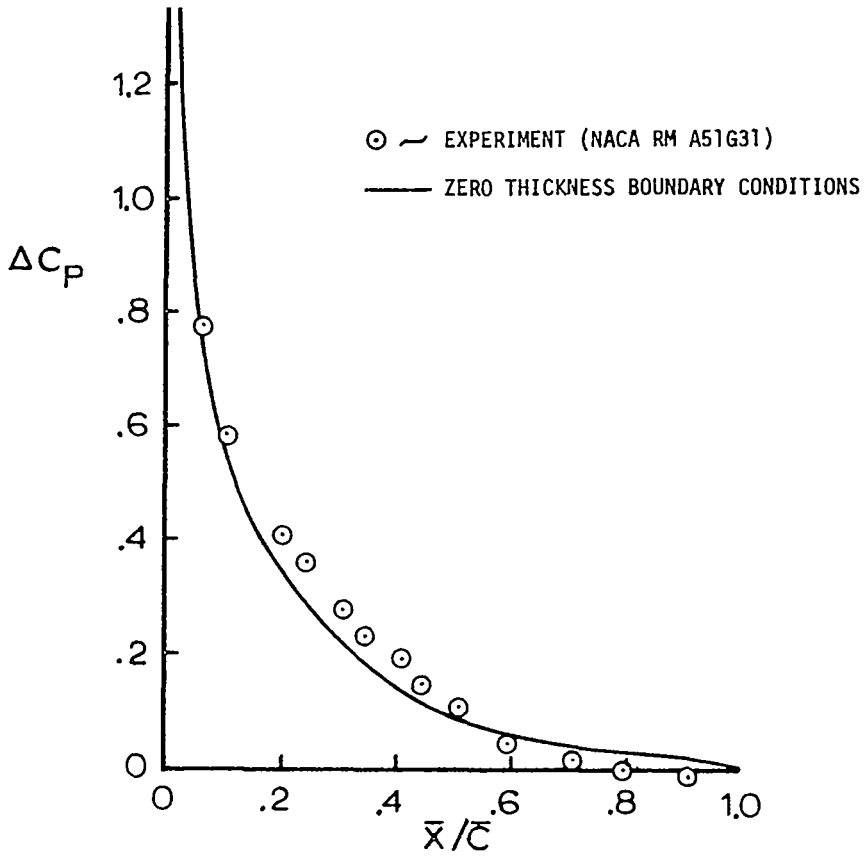

Figure 36.- Experimental and Zero Thickness Theoretical Pressure Distribution at y/s = 0.831, M = 0.80, α = 4°

The resulting theoretical pressure distribution was obtained using the standard linearized boundary conditions applicable for zero thickness lifting surfaces. It appears that a reasonable correlation is obtained on the average in that the theoretical distribution does approximate the experimental values in an average sense over the length of the streamwise chord. Theoretical pressures forward of the midchord are smaller than experimental values and are greater than experimental values for stations aft of the midchord.

The analysis was revised using a modification on the lifting surface boundary conditions such that the local velocity due to symmetrical thickness distribution is used instead of applying the uniform velocity distribution of a zero thickness lifting surface.

That is, the boundary condition of the integral equation was obtained from the definition

$$\bar{W}_j(x,y,o) = \frac{1}{V}\frac{Dz}{D\tau} = \frac{1}{V}\left[\frac{\partial z_j}{\partial \tau} + \frac{\partial z_j}{\partial x}\frac{\partial x}{\partial \tau}\right]$$

where z_j represents the displacement of the surface and is a function of time(τ).

$\frac{\partial z_j}{\partial x}$ ~ the slope of the surface at (x,y).

$\frac{\partial x}{\partial \tau}$ is usually taken to be equal to the remote velocity V, and for a zero thickness airfoil section this may be correct. However, physical experiments are conducted on finite thickness airfoil sections having local velocities that are not uniform over the chord length.

Consequently, the $\frac{\partial x}{\partial \tau}$ term should represent the local flow velocity V_{Local} at collocation stations in making a comparison between theoretical and real flow results.

The modified boundary conditions applicable to finite thickness airfoil sections are then defined as:

$$\bar{W}_j(x,y,o) = \frac{1}{V}\left[\frac{\partial z_j}{\partial \tau} + \frac{\partial z_j}{\partial x} V_{Local}\right]$$

V_{Local} is defined as being the steady streamwise velocity distribution that differs from V due to thickness effects only, and may be obtained from experimental results or by using the theoretical distributions of reference 17.

Theoretical results shown in figure 37 represent analyses using zero thickness and finite thickness boundary conditions and it is evident that in this case more accurate simulation of the physical flow results are obtained using local boundary conditions that incorporate finite thickness effects.

Theoretical pressure distributions forward of the midchord station approach the experimental values in a better fashion than do the results using zero thickness boundary conditions. Also, the theoretical distributions near the trailing edge predict the change in sign in pressures as indicated in the experimental results.

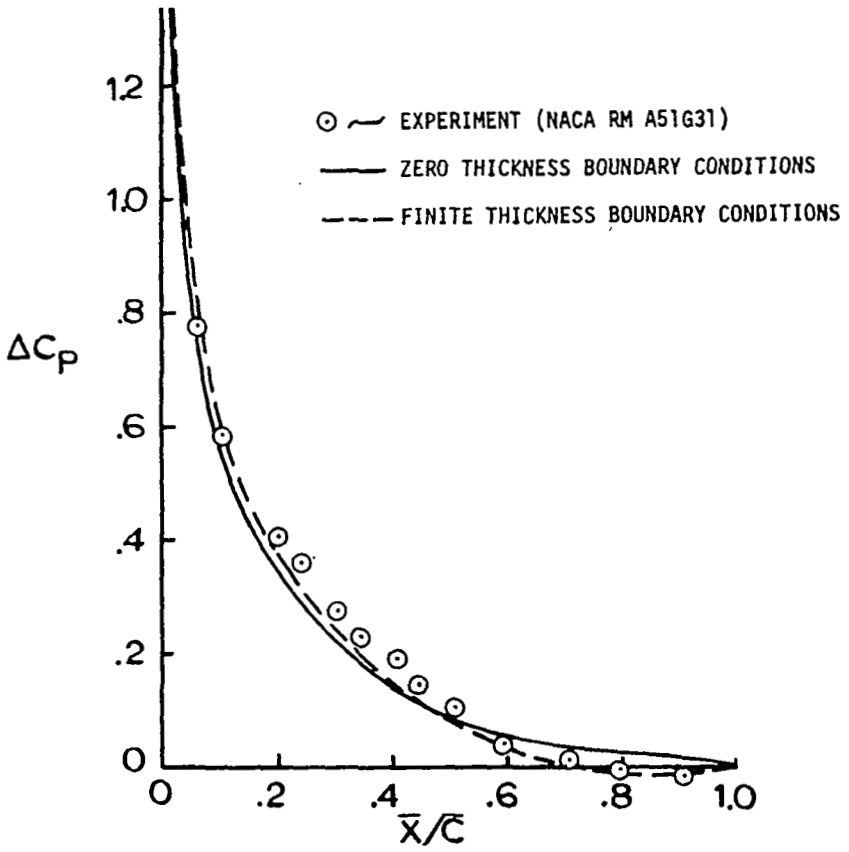

Figure 37.- Comparison of Pressure Distributions Predicted by Zero Thickness and Finite Thickness Boundary Conditions at a Semi-Span Station y/s = 0.831, for M = 0.80 and $\alpha = 4°$

Although no large changes in distributions are observed using modified boundary conditions, it does appear that the physical flow conditions are more accurately simulated and may contribute significantly to the design of energy absorbing Stability Augmentation Systems.

A program option is available for using modified boundary conditions within the analysis and the input data format along with limitations are given in section "3.7.2 LIMITATIONS" of reference 4.

NASA-Langley, 1972 — 1 CR-2003